Electronic Supplementary Material (ESI) for Journal of Materials Chemistry C.

Novel Donor Moiety 9,9,9′9′-tetramehtyl-9,9′10,10′-tetrahydro-2,10′-biacridine *Via* One-Pot C-H Arylation for TADF Emitters and Their Application in Highly Efficient Solution-Processable OLEDs

Yuchao Liu,[†‡▵] *Zheng Yin,*[†§▵] *Xiangbing Wang,*[†△] *Etienne Baranoff,*[#] *Di Zhou,*[†§]
Kai Zhang,[†] *Zhongjie Ren,*[‡*] *Shengyue Wang,*[†] *Weiguo Zhu,*[†*] *Yafei Wang*[†*]

Y. Liu, Z. Yin, X. Wang, D. Zhou, K. Zhang, G. Qian, S. Wang, Prof. W. Zhu, Prof. Y. Wang
National Experimental Demonstration Center for Materials Science and Engineering,
Jiangsu Key Laboratory of Environmentally Friendly Polymeric Materials,
Jiangsu Collaborative Innovation Center of Photovoltaic Science and Engineering,
Jiangsu Engineering Laboratory of Light-Electricity-Heat Energy-Converting Materials and Applications,
School of Materials Science & Engineering,
Changzhou University,
Changzhou 213164, China.
E-mail: zhuwg18@126.com; qiji830404@hotmail.com

Y. Liu, Prof. Z. Ren
State Key Laboratory of Chemical Resource Engineering,
College of Materials Science and Engineering,
Beijing University of Chemical Technology,
Beijing 100029, China
E-mail: renzj@mail.buct.edu.cn

Z. Yin, D. Zhou
College of Chemistry,
Xiangtan University,
Xiangtan 411105, China

Dr. E. Baranoff
Department of Chemistry
University of Birmingham
Birmingham, UK
B15 2TT

Abstract: 9,10-Dihydroacridine is a very popular donor unit for the construction of thermally activated delayed fluorescence (TADF) molecules due to its good electron-donating property and potential for chemical modifications. However, the functionalization of the 2/7-positions of the acridine unit has been rarely explored. In this contribution, the novel donor moiety 9,9,9′9′-tetramehtyl-9,9′10,10′-tetrahydro-2,10′-biacridine (BDMAc) was prepared *via* a one-pot C-H arylation procedure. The different acceptor fragments, diphenylsulfone (DPS), benzophenone (BPO) and 1,3,5-triazine (TRZ), were then introduced to synthesize three donor-acceptor molecules: DPS-BDMAc, BPO-BDMAc and TRZ-BDMAc. Single crystal X-ray diffraction and theoretical calculations show that these molecules possess the twisted molecular geometries and small energy gaps between the singlet and triplet excited states. All molecules exhibit TADF properties with the emission peaks between 480-600 nm in both solution and solid states, along with high emission efficiency of 69-89% in solid states. Solution-processed organic light-emitting diodes (OLEDs) based on these molecules were prepared with 25wt% dopant concentration. Although the devices showed the efficiency roll-off, a promising maximum EQE of ～23% and a luminance of 7173 cd m^{-2} was obtained for the BPO-BDMAc-based device. This research demonstrates the potential of this novel acridine group for the designing TADF molecules for efficient solution-processable OLEDs.

Keywords: Thermally activated delayed fluorescence, 9,9,9′9′-Tetramehtyl-9,9′10,10′-tetrahydro-2,10′-biacridine, Synthesis and property, Electroluminescence

1. Introduction

Since the seminal report by Tang and Vanslyke,[1] organic light-emitting diodes (OLEDs) have developed into fully functioning devices of great commercial interest, especially in display arena, due to its low driving voltage, high output efficiency, and the possibility to produce large area and flexible display.[2,3] Emissive materials, as the active layer in OLEDs, have been developed spanning from blue to near-infrared emissions.[4-6] There are three main categories of emissive materials, namely fluorescent, phosphorescent and thermally activated delayed fluorescence (TADF) materials. Owing to only harvesting the singlet excited states (S_1), fluorescent materials have stringent limitations for the efficient applications because of the intrinsic low internal quantum efficiency (*IQE*, ～25%).[7,8] Although phosphorescent materials can achieve 100% theoretical *IQE*,[9-11] the molecules containing heavy metal atom may be costly and environmentally harmful.

TADF materials have been reported as effective emitters for OLEDs by Adachi group and have since attracted a growing interest from academic and industrials.[12] Such material can harvest both S_1 and triplet excited (T_1) excitons through the reverse intersystem coupling (*r*ISC) process while being a metal-free chemical structure.[13] Over the past decade, great progress has been made for TADF materials and TADF-based OLEDs.[14-17] According to previous results,[18] a small energy gap (ΔE_{ST}) between S_1 and T_1 is a prerequisite for the TADF property, as it promotes the *r*ISC process. An effective molecular strategy to obtain the necessary small ΔE_{ST} is to realize the spatial separation between the highest occupied molecular orbital (HOMO) and lowest unoccupied molecular orbital (LUMO).[19] This can be achieved with a twisted donor-acceptor skeleton that decreases the overlap between HOMO and LUMO orbitals in turn reducing ΔE_{ST}.[20,21]

9,9-Dimethyl-9,10-dihydroacridine (DMAc) is a donor moiety widely used for TADF molecules because of its outstanding electron-donating ability and potential for functionalization.[22] According to a survey of Scifinder, more than 150 papers on DMAc-based TADF materials have been published between 2012 and 2019 (October). A large number of efficient OLEDs with high external quantum efficiency (*EQE*) were achieved based on DMAc-based TADF materials, using both small molecules and polymers.[23-27] For example, Kwon and Lee *et al.* reported the blue TADF material TDBA-Ac achieving a maximum *EQE* of 25.7% with CIE coordinate of (0.14, 0.15).[28] However, most of these reported devices are fabricated *via* vacuum deposition method, which is disadvantageous for cost-effectiveness and large-scale preparation.

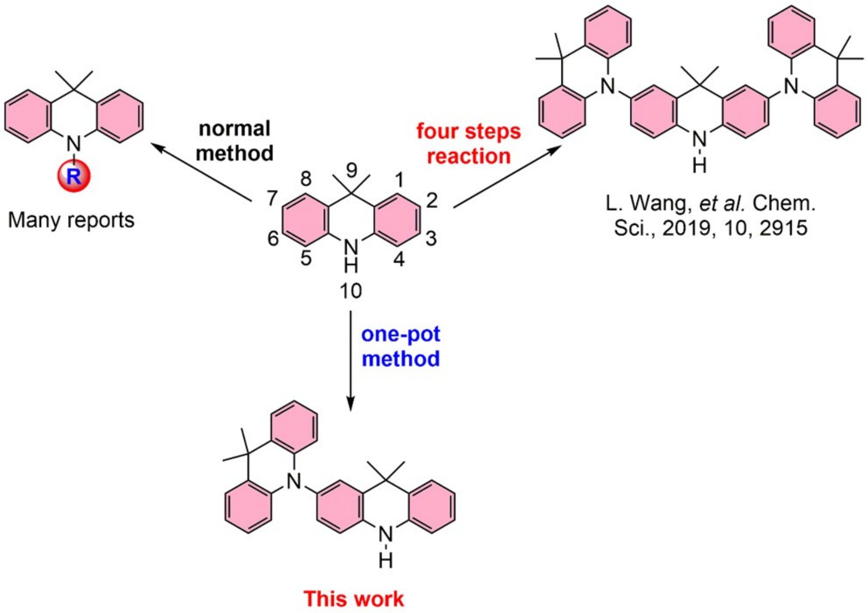

Chart 1. Numbering of the acridine chromophore and the structure evolutions of acridine derivatives.

The most common approach to the functionalization of the DMAc unit is to introduce substituents on the 10-position, that is on the nitrogen atom (**Chart 1**).[29,30] Very few researches focused on modifying other positions.[31-34] Recently, Wang′s group synthesized teracridine (**Chart 1**) *via* a four-steps procedure, including bromination, protection, coupling and deprotection reactions. The resulting TADF molecules using this novel teracridine donor moiety displayed a maximum *EQE* of 14.2% and luminance of 9689 cd m^{-2} in solution-processed OLEDs.[35] Although the synthetic method for this teracridine unit is demanding, TADF molecules bearing multiple acridine units are appealing due to their strong donor character and high solubility.

Herein we report a multi-acridine-based donor fragment obtained by a simple one-pot synthesis, and explore its application for solution-processed OLEDs. The novel unsymmetrical donor group 9,9,9′9′-tetramehtyl-9,9′10,10′-tetrahydro-2,10′-biacridine (BDMAc) was successfully prepared by one step in the presence of copper salts as catalyst. Subsequently combining BDMAc with diphenylsulfone, benzophenone and 1,3,5-triazine as the acceptor fragments, three TADF molecules were prepared and characterized. These molecules show emissions from sky-blue to green with high emission quantum yields (69~89%) in solid states. After optimization, satisfying device performance with the highest *EQE* of ~23% and luminance of 7173 cd m^{-2} was achieved for solution-processed OLEDs.

2. Results and Discussion

2.1. Synthesis and Characterization

The key precursor of 9,9,9′9′-tetramehtyl-9,9′10,10′-tetrahydro-2,10′-biacridine (BDMAc) was obtained by self-coupling of acridine *via* CuCl catalysis in toluene in the presence of potassium hydroxide and *o*-phenanthroline and isolated in 18% yield after purification by column chromatography. Compared to the previously reported teracridine derivatives needing multistep synthetic routes,[35] the presently reported BDMAc moiety requires only one-pot reaction, implying a cost-effective and efficient method. Importantly this reaction also presents opportunities for asymmetric designs by substituting the remaining 7-position of the main acridine moiety with various chemical groups for fine-tuning its photo- and electrochemical properties. A possible mechanism is proposed in **Scheme S1** to rationalize this Cu-catalyzed oxidative process.[36] First, CuCl with low oxidation state Cu(I) generates high oxidation state Cu(III) which reacts with the 9*H* of acridine to yield the intermediate A. Then the reaction between 7 (2)-C of another acridine and intermediate A provides the intermediate B, which finally undergoes reductive elimination to give BDMAc and Cu(I). The target D–A molecules were obtained *via* a typical Buchwald–Hartwig-coupling reaction in the presence of $Pd_2(dba)_3$ and $(^{t}Bu)_3P$ in toluene. All compounds were confirmed by ^1H NMR, ^{13}C NMR and TOF-MS. Excellent thermal stability has been observed for these molecules with the decomposition temperature (at 5% weight loss, T_d) above 400 °C (**Figure S1**).

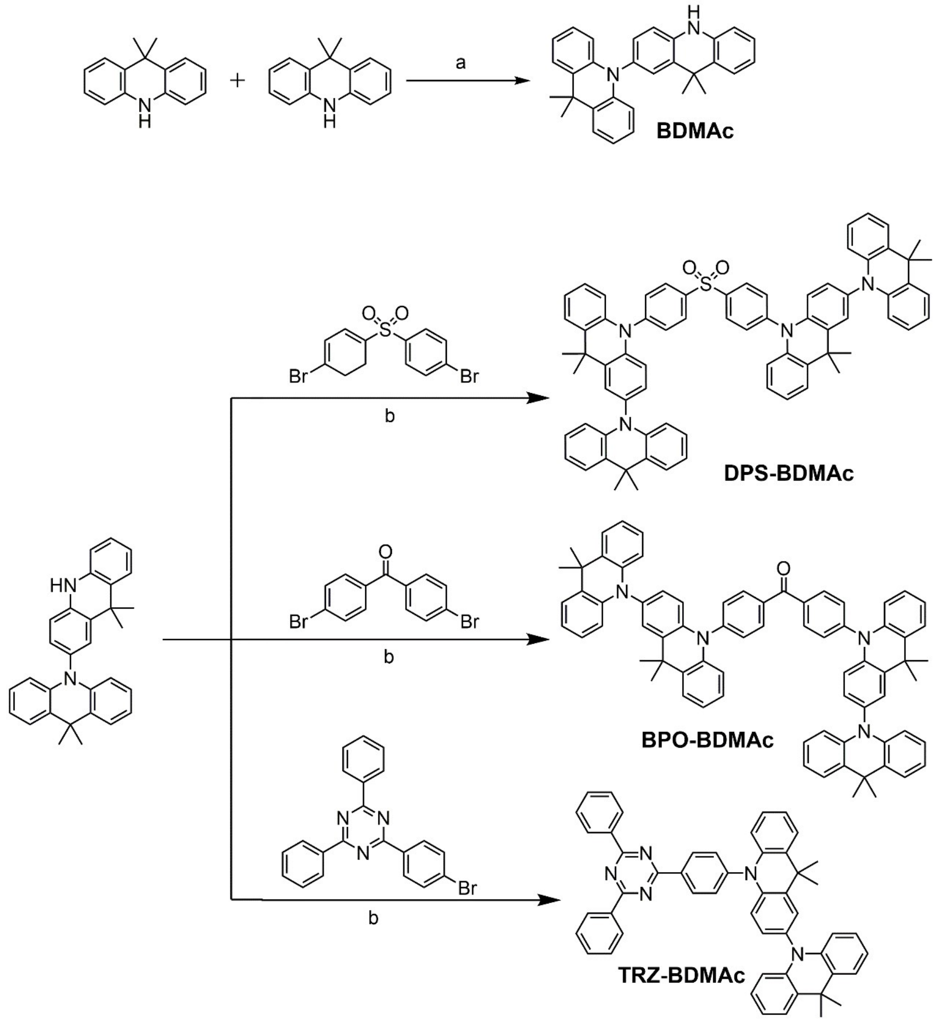

Scheme 1. Reaction conditions: a) CuCl, KOH, *o*-Phenanthroline, Toluene, reflux; b) $Pd_2(dba)_3$, $(^{t}Bu)_3P$, Toluene, reflux.

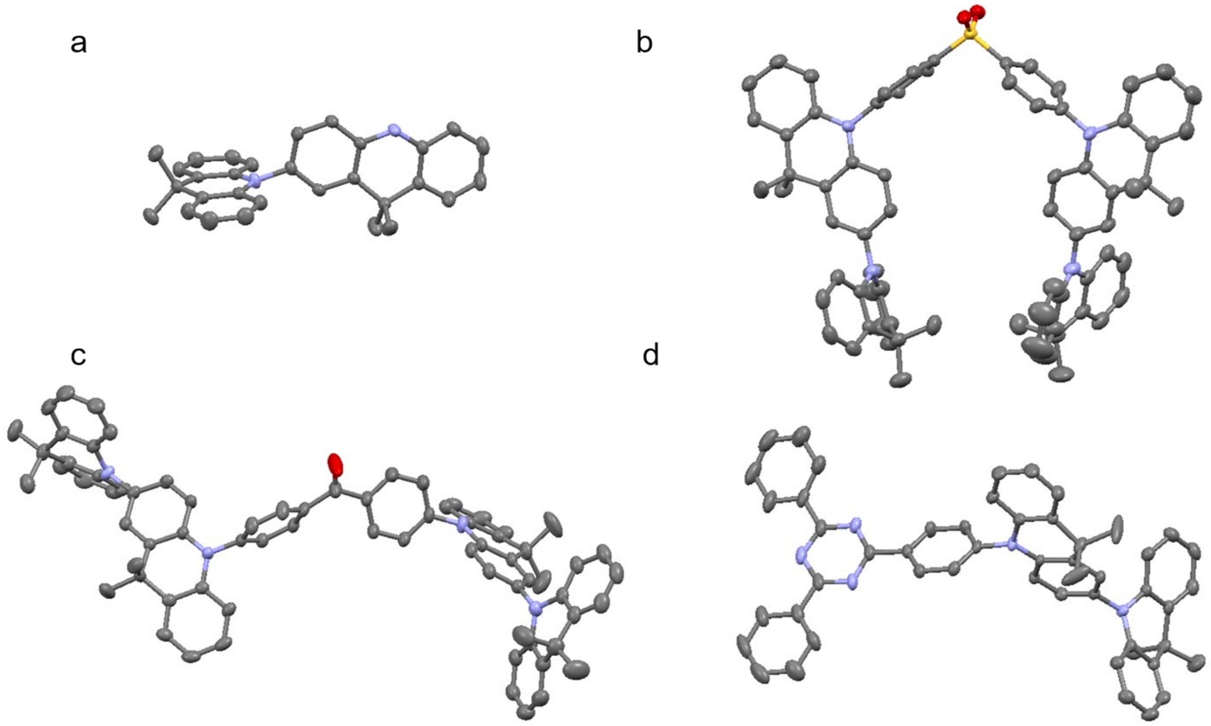

Figure 1. Single crystal structures of BDMAc and TADF compounds: (a) BDMAc; (b) DPS-BDMAc; (c) BPO-BDMAc; (d) TRZ-BDMAc. The display style is ellipsoid, and the probability level is 50%. The H atoms are omitted.

Single crystals of all molecules including the precursor BDMAc were achieved by slow evaporation from CH_2Cl_2/methanol solutions. The structures are shown in **Figure 1**, and the crystal parameters are listed in Supporting Information (**Table S1-S4**). BDMAc, DPS-BDMAc and BPO-BDMAc crystallize in a monoclinic system in the $P2_1/n$ space group, whereas TRZ-BDMAc crystallizes in a monoclinic crystal system in the C2/c space group. In the BDMAc crystal, the two acridine units have different molecular geometries. One acridine moiety shows little twisted structure with a dihedral angle (φ) of 174.46^o between both phenyl rings, while the other one is twisted with $\varphi = 163.79^o$. Importantly, both acridine fragments are almost orthogonal to another with a φ of 88.95^o, a feature that will promote electronic separation of the different active groups in the final molecules. As for the three emitters, the donor (BDMAc) and the acceptor units (DPS, BPO or TRZ) are also almost orthogonal, which is expected to result in a significant spatial separation of HOMO and LUMO. Due to the different twist angles of the two phenyl rings of DPS (104.66^o) and BPO (51.9^o), the crystals of DPS-BDMAc and BPO-BDMAc present distinct different molecular geometry. As for TRZ-BDMAc, the acceptor group TRZ exhibits a pseudo-planar structure. As shown in **Figure S2** the bond lengths between the nitrogen and carbon atom in the BDMAc fragment and the dihedral angles between benzene rings in acridine are directly different for these emitters. Obviously, the different electron-withdrawing groups play a significant role on the molecular geometry, which affect the photophysical properties of these emitters.

2.2. Theoretical calculation

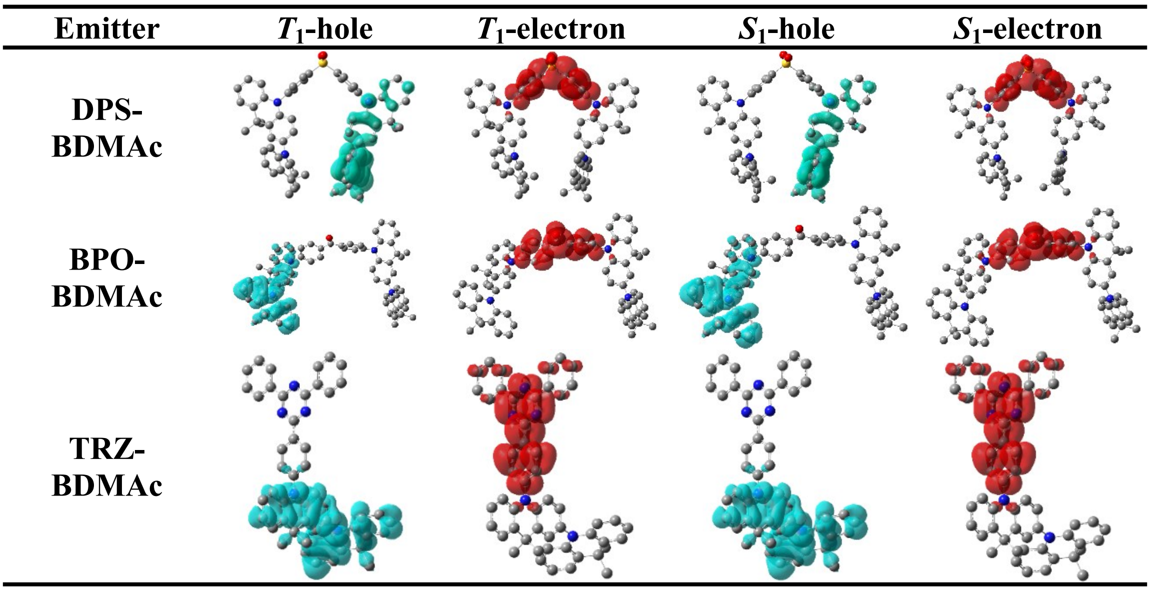

Figure 2. Natural Transition orbital (NTO) pairs for S_1 and T_1 of the TADF emitters.

Table 2. Calculated charge transfer and local excitation characters for the S_1 and T_1 states of the molecules

Emitter	S_1		T_1		SOCME (cm^{-1})	
	CT	LE	CT	LE	$\langle S_1 \| \hat{H}_{SO} \| T_1 \rangle$	$\langle S_1 \| \hat{H}_{SO} \| T_2 \rangle$
DPS-BDMAc	93.1	6.9	93.0	7.0	0	0.037
BPO-BDMAc	99.0	1.0	99.0	1.0	0	0
TRZ-BDMAc	99.8	0.2	98.3	1.7	0	0.800

To explore the relationship between the electronic nature of the frontier orbitals and the TADF properties of the molecules, density functional theoretical (DFT) and time-dependent DFT (TD-DFT) calculations were performed via Gaussian 09 program with b3lyp/6-31g (d) method. As depicted in **Figure S3**, the HOMOs of these emitters are mainly localized on the BDMAc moiety, whereas the LUMOs are distributed on the acceptor fragment. Compared to the molecules with DMAc unit,[37-39] clear contributions from the second acridine moiety are observed for the HOMOs in compounds DPS-BDMAc, BPO-BDMAc and TRZ-BDMAc. Obviously, the biacridine unit has an obvious effect on the HOMO due to the increased donor property. As shown in **Figure 2**, the HOMO and LUMO present the distinct special separation, accompanied with a relatively small spatial overlap on the *N*-heterocycle moiety, possibly underpinning efficient light emission. Furthermore, the ΔE_{ST} of all molecules are very small, approximately 0.003 eV, which is favorable to the realization of *r*ISC process.

To further clarify the character of excited states in these TADF emitters, quantum-chemical calculations were performed using Gaussian 09, and the electron excitations were analyzed via Multiwfn 3.6. As shown in **Figure 2**, the distributions of hole and electron densities for all molecules are strongly localized on the donor and acceptor moieties, respectively, indicating the charge transfer (CT) nature of both the singlet (S_1) and the triplet excited (T_1) states. To explore the contribution of local excitations (LE) to the emitting excited states, the integral of Sr function was investigated by further exploiting the excited-state wave functions of these three molecules. The SOC matrix elements (SOCME) for all molecules were calculated using the ORCA 4.1.1 package. B3LYP/G 6-31g(d) was employed for the electronic structure calculations, and five excited states were considered in SOCME calculation (**Table 2**). Based on the calculation results, it can be concluded that the SOC effect can hardly enhance the RISC process in our case because both the S_1 and T_1 states have the absolutely dominant CT characters.[40,41]

2.3. Photophysical property

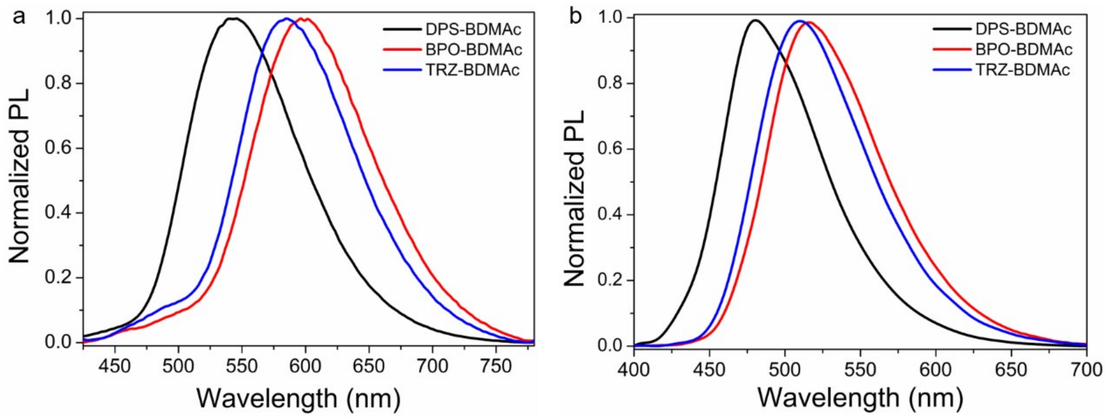

Figure 3. PL spectra of compounds: (a) in toluene solution (10^{-5} M); (b) 10 wt% molecules in doped mCPCN.

Table 1. photophysical data of TADF emitters

	$^{a}\lambda_{abs}$ (nm)	λ_{em} (nm)	$^{b}\tau_P/\tau_D$ (ns)	$^{b}\Phi$ (%)	ΔE_{ST} (eV)	$^{c}E_{HOMO}$ (eV)	$^{c}E_{LUMO}$ (eV)	T_d (^{o}C)
DPS-BDMAc	289, 370	^{a}543	32.6	69.1	0.02	-5.11	-2.12	430
		^{b}481	2100					
BPO-BDMAc	290, 392	^{a}600	44.9	89.1	0.03	-5.16	-2.34	433
		^{b}516	3000					
TRZ-BDMAc	283, 390	^{a}585	36.5	87.0	0.04	-5.38	-2.56	400
		^{b}510	2800					

a: Measured in toluene solution; b: measured in doped films; c: measured in CH_3CN solution. $V_{ox,Fc/Fc+} = 0.44$ V, $E_{LUMO} = E_{HOMO}-E_{opt}$

All compounds show two clear absorption bands in toluene (10^{-5} M) between 250 nm and 500 nm (**Figure S4**). Based on the absorption spectra of previously reported TADF emitters,[42] the intense absorption bands at short wavelength (*ca.* 286 ± 3 nm) are assigned to transitions localized on donor fragments, whereas the weak absorption bands at the longer wavelength originate from intramolecular charge transfer (ICT) transitions between the donor and the acceptor units. From the absorption edge in **Figure S4**, it is found that the optical energy gaps decrease in the order DPS-BDMAc>TRZ-BDMAc>BPO-BDMAc. This phenomenon indicates that the different acceptor strengths can clearly affect the ground states.

Upon excitation at 360 nm (ICT band) at room temperature, DPS-BDMAc, TRZ-BDMAc and BPO-BDMAc display broad and unresolved emission spectra peaking at 543, 585 and 600 nm in toluene, respectively (**Figure 3a**). The structureless emissions support the charge transfer (CT) nature of the excited states. Compared to the emissions from solutions, PL spectra from doped solid films (25 wt% in mCPCN) are significantly blue-shifted (**Figure 3b** and **Table 1**). Two factors can be responsible for this variation:[43] (i) the restriction of molecular motions in the solid states; (ii) the polarity of mCPCN. Importantly, an effective energy transfer between mCPCN and the TADF emitters is most likely to take place because of the absence of emission from the host material. Compared to the analogous acridine-based compounds[37-39] (**Table S5**), BDMac-based compounds have clearly red-shifted emission spectra due to the increased donor property, leading to stronger ICT effect. In the doped films under N_2 atmosphere, all compounds possess high photoluminescent quantum efficiency (Φ_{PL}) of 69% for DPS-BDMAc, 89% for BPO-BDMAc and 87% for TRZ-BDMAc.

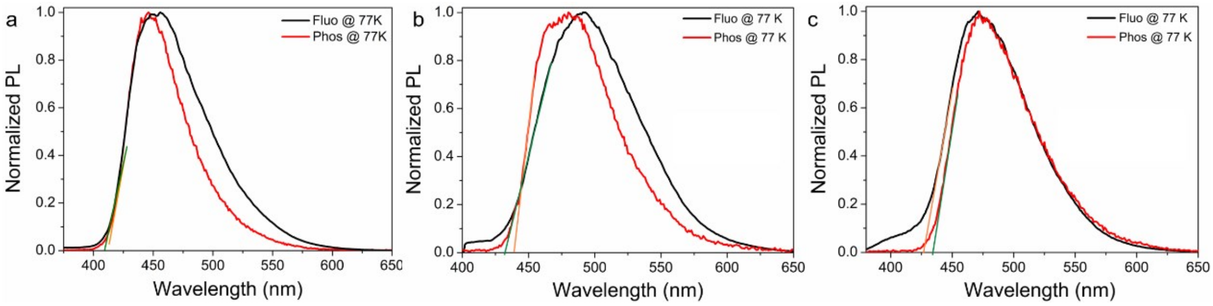

Figure 4. Low temperature PL and phosphorescence (recorded at 77 K) spectra of (a) DPS-BDMAc, (b) BPO-BDMAc, (c) TRZ-BDMAc in *m*CPCN.

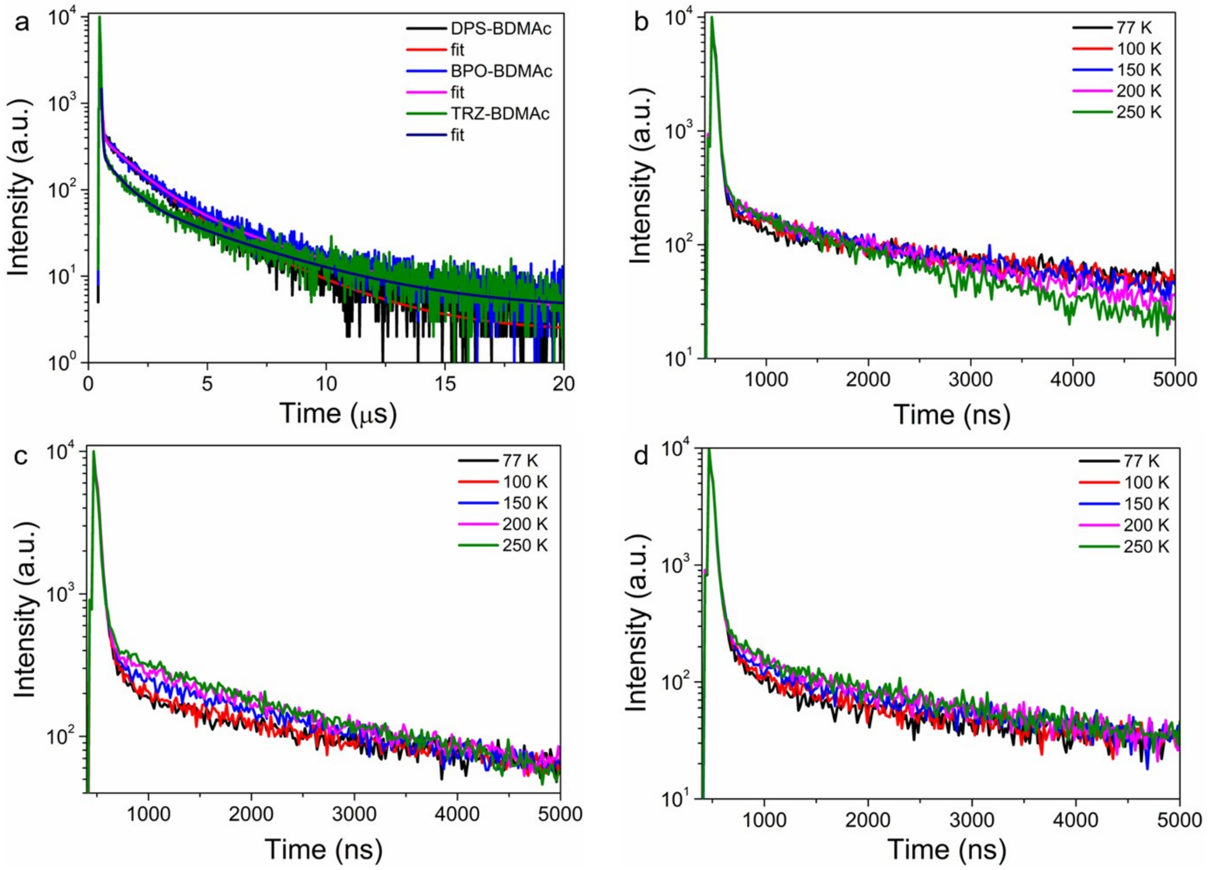

Figure 5. Emission lifetime profiles of 10 wt% of molecules doped in mCPCN at room temperature (a) and different temperatures (b: DPS-BDMAc; c: BPO-BDMAc and d: TRZ-BDMAc)

Table 3. Photophysical data of the TADF emitters

Emitters	τ_p/Φ_p [ns/%]	τ_d/Φ_d [μs/%]	PLQY [%]	k_p [10^7 s^{-1}]	k_d [10^5 s^{-1}]	k_{ISC} [10^7 s^{-1}]	K_{rISC} [10^6 s^{-1}]	k_r [10^6 s^{-1}]	k_{nr} [10^6 s^{-1}]
DPS-BDMAc	32.6/15.4	2.1/63.7	69.1	3.07	4.76	2.83	2.136	4.72	2.11
BPO-BDMAc	44.9/10.1	3.0/79.1	89.1	2.22	3.33	1.98	2.924	2.25	0.28
TRZ-BDMAc	36.5/16.3	2.8/70.7	87.0	2.74	3.57	2.23	1.903	4.47	0.67

According to the onset of phosphorescent and fluorescent spectra,[44] the differences between low temperature (77 K) fluorescence and phosphorescence demonstrate the very small ΔE_{ST} values for all molecules (0.02～0.04 eV, **Figure 4**), in line with theoretical calculations. As shown in **Table S5**, BDMAc-based compounds show narrow ΔE_{ST} than that of DMAc-based compounds in previous reports,[37-39] implying BDMAc moiety could play a positive role on the rISC process. To confirm the TADF process, transient PL decay was measured for all molecules in doped mCPCN. As shown in **Figure 5a**, the distinct second-order exponential decays with both prompt and delayed emission components were detected in all cases. The prompt (delayed) components with lifetimes of 32.6 ns (2.1 μs), 44.9 ns (3.0 μs) and 36.5 ns (2.8 μs) were obtained for DPS-BDMAc, BPO-BDMAc and TRZ-BDMAc respectively. Then the temperature-dependent transient decay curves were further measured in the doped films (**Figure 5b-5d**). It appears that the proportion of delayed component increases concomitantly with the temperature from 77 to 250 K, which is ascribed to the acceleration of the reverse intersystem coupling from T_1 to S_1 state. This result demonstrates that all molecules display TADF emission.[45,46] Interestingly, it is noted that the compound DPS-BDMAc showed a clearly decreased trend with the increased temperatures in the large scale (**Figure 5b**), probably implying the phosphorescence of the acceptor involving in the delay components.[47,48] Based on the Φ_{PL} and lifetime, the photophysical constants were calculated according to the formulae (S1)～(S6) (Supporting Information). As listed in **Table 3**, all compounds possess high k_{rISC} values in the order of 10^6 s^{-1}. BPO-BDMAc exhibits the highest k_{rISC} and the lowest k_{nr}, with the rISC process being about 10 times more effective than the non-radiative decay. TRZ-BDMAc is also an efficient emitter, yet the k_{rISC} is the lowest of the three molecules, in line with it having the largest ΔE_{ST} value. In addition, both k_r and k_{nr} are double to those of BPO-BDMAc, which may be attributed to the different numbers of donor units. DPS-BDMAc displays the lowest emission quantum yield, which can be attributed to the high k_{nr} value, almost one order of magnitude larger than that of the other two emitters.

2.4. Electrochemical properties

The electrochemical properties of three TADF emitters were carefully explored through cyclic voltammetry (CV) in degassed CH_3CN solution. The CV curves are shown in **Figure S5** and the relevant data are listed in **Table 1**. Only quasi-reversible oxidation wave at 0.75 (*vs*. Fc/Fc$^+$, the same below), 0.80 and 1.02 V were observed for DPS-BDMAc, BPO-BDMAc and TRZ-BDMAc, respectively. According to the empirical formula of $E_{\mathrm{HOMO}} = -(E_{\mathrm{OX}} + 4.8)$ eV, the HOMO energy level is -5.11 eV for DPS-BDMAc, -5.16 eV for BPO-BDMAc and -5.38 eV for TRZ-BDMAc. As expected, both DPS-BDMAc and BOP-BDMAc show a shallower HOMO energy than TRZ-BDMAc, owing to the two BDMAc fragments imparting a stronger donor character. Based on the HOMO energy level and the optical energy gap (E^{opt}), the LUMO energy levels are evaluated to be -2.12, -2.34 and -2.56 eV for DPS-BDMAc, BPO-BDMAc and TRZ-BDMAc, respectively.

2.5. Electroluminescence properties

To assess the electroluminescence (EL) properties of the TADF emitters, the devices with a configuration of ITO/PEDOT:PSS (40nm)/mCPCN: emitters (25 wt%, 45 nm)/DPEPO (10nm)/TmPyPB (40nm)/Liq (1.2nm)/Al (120 nm) were fabricated *via* a solution-process method. In this device structure, PEDOT:PSS is poly(3,4-ethylenedioxythiophene):poly(styrene sulfonate), which acts as the hole injecting layer. In view of its large triplet energy and excellent bipolar transport property,[4,49] 9-(3-(9H-carbazol-9-yl)phenyl)-9H-carbazole-3-carbonitrile (*m*CPCN) was used as the host matrix. The emitting layer is a blend of *m*CPCN and TADF molecules, in which the dopant concentration is 25 wt%. DPEPO [bis(2-(diphenylphosphino)phenyl)ether oxide] and TmPyPB [1,3,5-tri(m-pyrid-3-ylphenyl)benzene] are used as the hole-blocking and electron-transporting layer, respectively. The molecular structure of the materials in these devices and the relevant energy level diagrams are listed in **Figure S6**. The EL data are summarized in **Table 4**.

As shown in **Figure 6a**, the devices show intense EL emission with the maximum emission peaks at 498 nm, 522 nm and 516 nm for DPS-BDMAc, BPO-BDMAc and TRZ-BDMAc, respectively. Compared to the PL spectra of doped films, the almost identical EL spectra demonstrate that the excitons are well confined in the emitter layer. In addition, the absence of electroluminescence from *m*CPCN further supports an effective energy transfer between the host matrix and the TADF molecules. The corresponding Commission International de l′Éclairage (CIE) coordinates are (0.23, 0.40) for DPS-BDMAc, (0.29, 0.54) for BPO-BDMAc and (0.27, 0.51) for TRZ-BDMAc based device (**Figure S7**).

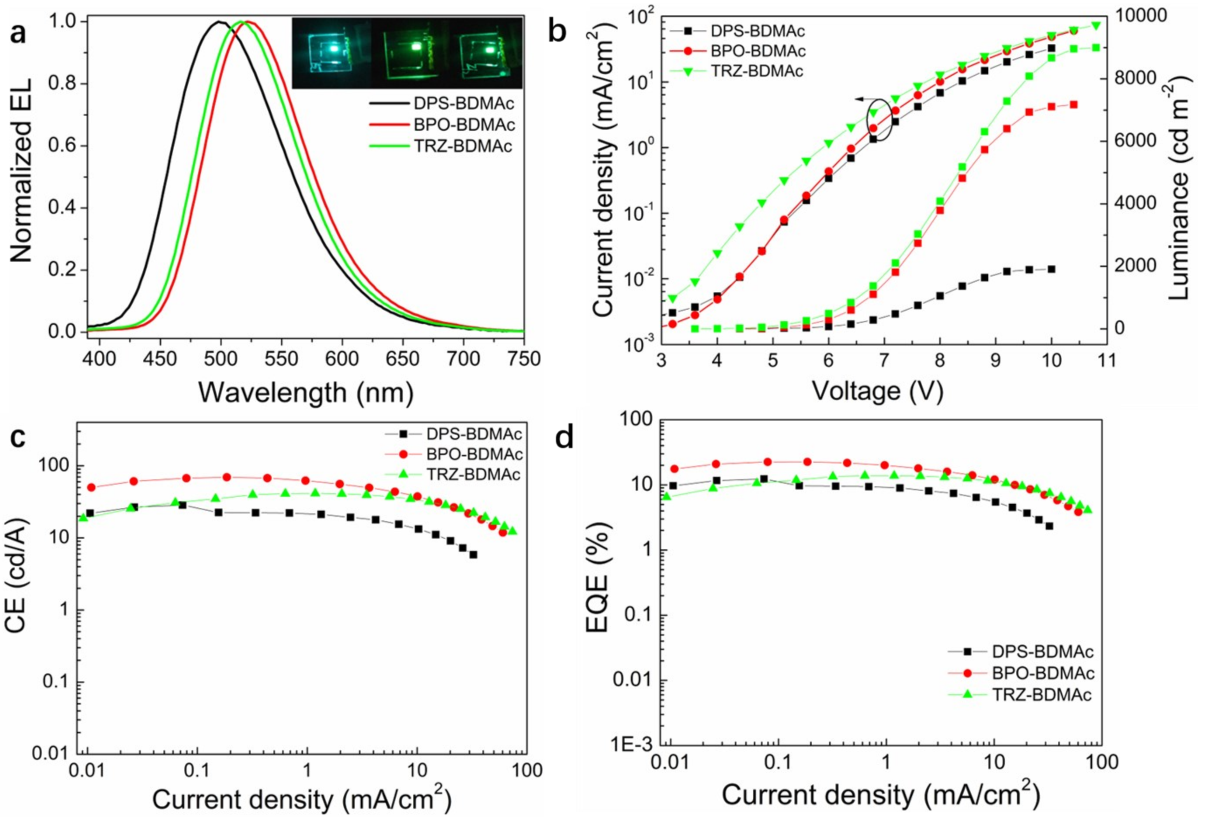

Figure 6. Devices characters based on Liq/Al cathode. (a): EL spectra, the photographs of the devices are DPS-BDMAc, BPO-BDMAc and TRZ-BDMAc from left to right, respectively; b) J-V-L curves; c) *CE*-current density curves; d) *EQE*-current density curves.

Table 4. EL data for the TADF emitters-based devices

	Dopant /wt %	**V_{on} /V**	**L_{max} /cd m^{-2}**	**CE_{max} /cd A^{-1}**	**EQE_{max} /%**	***CIE* (x, y)**	**λ /nm**
DPS-BDMAc	25	4.4	1904	28.42	12.35	(0.23, 040)	498
BPO-BDMAc	25	4.4	7173	69.25	22.53	(0.29, 0.54)	522
TRZ-BDMAc	25	3.6	8994	41.44	13.86	(0.27, 0.51)	516

Current density-voltage-luminance plots (*J-V-L*), current efficiency (*CE*)-current density curves and external quantum efficiency (*EQE*)-current density characteristics are shown in **Figure 6b～6c**, respectively. All devices show a fairly low turn-on voltage (V_{on}, at 1 cd m^{-2})

in the range of 3.6～4.4 V. The blue-greenish device based on DPS-BDMAc presented a maximum *EQE* of 12.35%, *CE* of 28.42 cd A^{-1} and luminance of 1904 cd m^{-2}. Conversely, the green-emitting devices based on BPO-BDMAc and TRZ-BDMAc possess better performances than that of the DPS-BDMAc based device, in line with their PLQY in solid states. A maximum *EQE* of 22.53% and 13.86%, *CE* of 69.25 cd A^{-1} and 41.44 cd A^{-1} and luminance of 7173 cd m^{-2} and 8994 cd m^{-2} for BPO-BDMAc and TRZ-BDMAc based devices, respectively. It is noted that BPO-BDMAc based device possesses a best performance because of its highest PLQY and k_{rISC} value among of them. Unfortunately, these devices display a unsatisfied luminance which could be ascribed to the device configuration. Although the performances lag behind that of device fabricated by thermal vacuum evaporation, it is among the best results reported for the solution processable devices without any outcoupling features.

3. Conclusion

In summary, a novel donor unit 9,9,9′9′-tetramehtyl-9,9′10,10′-tetrahydro-2,10′-biacridine was prepared by one-pot procedure and used for the construction of three TADF emitters. Compared to the acridine unit, BDMAc group has an important role on the HOMO energy, energy difference gap and solubility. Introduction of acceptor units DPS, BPO and TRZ, all three molecules exhibit clear TADF emission with high efficiency of 69-89% in solid states. The different acceptor fragments used in the TADF molecules allow for the tuning of emitted lights from sky-blue to green. Employing these TADF molecules as the emitting dopants, solution-processed devices showed the attractive performance with a maximum EQE of ～23% based on BPO-BDMAc. The straightforward synthetic method for designing novel donor could be very charming for TADF molecules in high efficiency solution-processable OLEDs.

4. Experimental Section

Synthesis *of compound BDMAc:* A mixture of 9,9-dimethyl-9,10-dihydroacridine (600 mg, 2.97 mmol), CuCl (44 mg, 0.445 mmol), *o*-phenanthroline (160 mg, 0.89 mmol), KOH (166 mg, 2.97 mmol) and 40 mL toluene were heated to 120 $^{\circ}C$ and stirred for 24 h under a nitrogen atmosphere. After cooling to room temperature, the mixture was extracted with dichloromethane (CH_2Cl_2, 3×30 mL). The combined organic layers were washed with water, dried over anhydrous $MgSO_4$ and evaporated to dryness. The residue was purified by column chromatography (petroleum ether/CH_2Cl_2 = 5:1 v/v) to give compound BDMAc as a light yellow solid (120 mg, yield 19%). ^1H NMR (300 MHz, DMSO-d^6) δ 9.17 (s, 1H), 7.47-7.44 (m, 2H), 7.37 (d, J = 9.0 Hz, 1H), 7.24 (d, J = 3.0 Hz, 1H), 7.13-7.04 (m, 2H), 7.00-6.92 (m, 3H), 6.88-6.82 (m, 4H), 6.23-6.20 (m, 2H), 1.61 (s, 6H), 1.49 (s, 6H).

Synthesis of DPS-BDMAc: A mixture of compound BDMAc (255 mg, 0.612 mmol), 1-bromo-4-((4-bromocyclohexa-1,3-dien-1-yl)sulfonyl)benzene (100 mg, 0.266 mmol), ^{t}BuONa (102 mg, 1.06 mmol), $Pd_2(dba)_3$ (14.6 mg, 15.9 μmol), $(^tBu)_3P$ (6.46 mg, 31.9 μmol) and 60 mL toluene was stirred at 120 °C for 24 h under a nitrogen atmosphere. After cooling to room temperature, the mixture was extracted with dichloromethane (CH_2Cl_2, 3×30 mL). The combined organic layers were washed with water, dried over anhydrous $MgSO_4$ and evaporated to dryness. The residue was purified by column chromatography (petroleum ether/CH_2Cl_2 = 2:1 v/v) to give the compound DPS-BDMAc as a green solid (100 mg, 36%).^1H NMR (300 MHz, $CDCl_3$) δ 8.37-8.32 (m, 4H), 7.73-7.67 (m, 4H), 7.52-7.47 (m, 2H), 7.45 (d, J = 1.7 Hz, 2H), 7.43 (d, J = 1.9 Hz, 2H), 7.39 (d, J = 2.3 Hz, 2H), 7.08-6.99 (m, 4H), 6.98-6.86 (m, 10H), 6.52 (d, J = 8.6 Hz, 2H), 6.36-6.32 (m, 2H), 6.28 (dd, J = 7.9, 1.5 Hz, 4H), 1.67 (d, J = 7.5 Hz, 24H). ^{13}C NMR (126 MHz, CDCl3) δ 146.44, 141.15, 140.64, 140.17, 139.87, 134.56, 133.96, 131.68, 130.95, 130.74, 129.86, 128.95, 127.95, 126.53, 125.27, 122.08, 120.37, 116.46, 114.78, 113.91, 36.46, 35.96, 31.44, 30.49, 22.65, 14.13. TOF-MS (ESI) m/z calcd for $C_{72}H_{62}N_4O_2S$: 1046.46; $[M+H]^+$ found: 1047.28.

Synthesis of BPO-BDMAc: The synthesis procedure is similar with that of DPS-BDMAc. The residue was purified by column chromatography (petroleum ether/CH_2Cl_2 = 3:1 v/v) to give the compound BPO-BDMAc as a yellow solid (200 mg, 67%). ^1H NMR (300 MHz, $CDCl_3$) δ 8.24 (d, J = 9.0 Hz, 4H), 7.66 (d, J = 9.0 Hz, 4H), 7.53-7.50 (m, 2H), 7.47-7.44 (m, 4H), 7.40 (d, *J* = 3.0 Hz, 2H), 7.09-7.03 (m, 4H), 7.01-6.88 (m, 10H), 6.58 (d, *J* = 9.0 Hz, 2H), 6.45-6.41 (m, 2H), 6.35-6.32 (m, 4H), 1.70 (s, 24H). ^{13}C NMR (101 MHz, $CDCl_3$) δ 195.23, 145.85, 141.69, 140.90, 140.64, 137.47, 134.58, 133.68, 133.25, 131.76, 130.74, 130.31, 129.32, 128.30, 127.14, 126.83, 125.72, 122.09, 120.78, 116.56, 114.90, 114.46, 36.87, 36.40, 31.96, 31.16. TOF-MS (ESI) m/z calcd for $C_{73}H_{62}N_4$: 1010.49; $[M+H]^+$ found: 1011.39.

Synthesis of TRZ-BDMAc: The synthesis procedure is similar with that of DPS-BDMAc. The residue was purified by column chromatography (petroleum ether/CH_2Cl_2 = 5:1 v/v) to give compound TRZ-BDMAc as a light green solid (89 mg, 48%). ^{1}H NMR (400 MHz, $CDCl_3$) δ 9.08 (d, *J* = 8.0 Hz, 2H), 8.84-8.82 (m, 4H), 7.69-7.59 (m, 8H), 7.53-7.51 (m, 1H), 7.46-7.44 (m, 2H), 7.40 (d, *J* = 2.3 Hz, 1H), 7.08-6.97 (m, 4H), 6.93-6.89 (m, 3H), 6.61 (d, *J* = 8.0 Hz, 1H), 6.47-6.45 (m, 1H), 6.36 (d, *J* = 8.0 Hz, 2H), 1.72 (s, 12H). ^{13}C NMR (125 MHz, $CDCl_3$) δ 172.04, 171.17, 145.14, 141.42, 140.78, 140.52, 136.60, 136.19, 133.98, 132.88, 131.85, 131.70, 130.08, 129.97, 129.18, 128.88, 127.88, 126.83, 126.54, 125.40, 121.50, 120.41, 116.15, 114.53, 114.20, 77.16, 36.52, 36.08, 31.66, 30.95. TOF-MS (ESI) m/z calcd for $C_{51}H_{41}N_5$: 723.34; $[M+H]^+$ found: 724.32.

Acknowledgements

Y. Liu, Z. Yin and X. Wang contributed equally to this work. Financial support was from the National Natural Science Foundation of China (51773021, 51911530197, U1663229, 51922021), Six talent peaks project in Jiangsu Province (XCL-102), the Talent project of Jiangsu Specially-Appointed Professor, Natural Science Fund for Colleges and Universities in Jiangsu Province (No. 19KJA430002).

References

1 C. Tang and S. VanSlyke, *Appl. Phys. Lett.*, 1987, **51**, 913-915.

2 D. Zhang, T. Huang and L. Duan, *Adv. Mater.*, 2019, 1902391.

3 Y. Liu, C. Li, Z. Ren, S. Yan and M. R. Bryce. *Nat. Rev. Mater.*, 2018, **3**, 18020-18039.

4 T. Lin, T. Chatterjee, W. Tsai, W. Lee, M. Wu, M. Jiao, K. Pan, C. Yi, C. Chung, K. Wong and C. Wu, *Adv. Mater.*, 2016, **28**, 6976-6983.

5 T. Wu, M. Huang, C. Lin, P. Huang, T. Chou, R. Chen-Cheng, H. Lin, R. Liu and C. Cheng, *Nat. Photonics*, 2018, **12**, 235-240.

6 W. Zeng, H. Lai, W. Lee, M. Jiao, Y. Shiu, C. Zhong, S. Gong, T. Zhou, G. Xie, M. Sarma, K. Wong, C. Wu and C. Yang, *Adv. Mater.*, 2018, **30**, 1704961.

7 M. Baldo, D. O'brien, Y. You, A. Shoustikov, S. Sibley, M. Thompson and S. Forrest, *Nature*, 1998, **395**, 151-153.

8 D. Kondakov, *J. Soc. Inf. Display*, 2009, **17**, 137-144.

9 C. Adachi, M. Baldo, M. Thompson and S. Forrest, *J. Appl. Phys.*, 2001, **90**, 5048-5051.

10 C. Lee and J. Lee, *Adv. Mater.*, 2013, **25**, 5450-5454.

11 B. Minaev, G. Baryshnikov and H. Agren, *Phys. Chem. Chem. Phys.*, 2014, **16**, 1719-1758.

12 A. Endo, M. Ogasawara, A. Takahashi, D. Yokoyama, Y. Kato and C. Adachi, *Adv. Mater.*, 2009, **21**, 4802-4806.

13 Q. Zhang, B. Li, S. Huang, H. Nomura, H. Tanaka and C. Adachi, *Nat. Photonics*, 2014, **8**, 326-332.

14 Y. Tao, K. Yuan, T. Chen, P. Xu, H. Li, R. Chen, C. Zheng, L. Zhang and W. Huang, *Adv. Mater.*, 2014, **26**, 7931-7958.

15 M. Wong and E. Zysman-Colman, *Adv. Mater.*, 2017, **29**, 1605444.

16 Q. Wei, Z. Ge and B. Voit, *Macromol. Rapid Commun.*, 2019, **40**, 1800570.

17 Y. Zou, S. Gong, G. Xie and C. Yang, *Adv. Optical Mater.*, 2018, **6**, 1800568-1800592.

18 H. Uoyama, K. Goushi, K. Shizu, H. Nomura and C. Adachi, *Nature*, 2012, **492**, 234-238.

19 T. Ziegler, A. Rauk and E. Baerends, *Chim. Acta.*, 1977, **43***,* 261-271.

20 Q. Zhang, H. Kuwabara, W. Potscavage, S. Huang, Y. Hatae, T. Shibata and C. Adachi, *J. Am. Chem. Soc.* 2014, **136**, 18070-18081.

21 D. Lee, M. Kim, S. Jeon, S. Hwang, C. Lee and J. Lee, *Adv. Mater.* 2015, **27***,* 5861-5867.

22 S. Reddy, V. Sree, K. Gunasekar, W. Cho, Y. Gal, M. Song, J. Kang and S. Jin, *Adv. Optical Mater.*, 2016, **4**, 1236-1246.

23 Q. Zhang, D. Tsang, H. Kuwabara, Y. Hatae, B. Li, T. Takahashi, S. Lee, T. Yasuda and C. Adachi, *Adv. Mater.*, 2015, **27**, 2096-2100.

24 W. Tsai, M Huang, W. Lee, Y. Hsu, K. Pan, Y. Huang, H. Ting, M. Sarma, H. Hu, C. Chen, M. Lee, K. Wong and C. Wu, *Chem. Commun.*, 2015, **51**, 13662-13665.

25 S. Lee, T. Yasuda, H. Komiyama, J. Lee and C. Adachi, *Adv. Mater.*, 2016, **28**, 4019-4024.

26 Y. Wada, S. Kubo and H. Kaji, *Adv. Mater.*, 2018, **30**, 1705641-1705648.

27 C. Li, Z. Ren, X. Sun, H. Li and S. Yan, *Macromolecules*, 2019, **52**, 2296-2303.

28 D. Ahn, S. Kim, H. Lee, I. Ko, D. Karthik, J. Lee and J. Kwon, *Nat. Photonics*, 2019, **13**, 540-546.

29 S. Reddy, W. Cho, V. Sree and S. Jin, *Dyes Pigm.*, 2016, **134**, 315-324.

30 S. Shao, J. Hu, X. Wang, L. Wang, X. Jing and F. Wang, *J. Am. Chem. Soc.*, 2017, **139**, 17739-17742.

31 H. Higginbotham, C. Yi, A. Monkman and K. Wong, *J. Phys. Chem. C*, 2018, **122**, 7627-7634.

32 P. Pandit, K. Yamamoto, T. Nakamura, K. Nishimura, Y. Kurashige, T. Yanai, G. Nakamura, S. Masaoka, K. Furukawa, Y. Yakiyama and M. Kawano, *Chem. Sci.*, 2015, **6**, 4160-4173.

33 W. Zeng, T. Zhou, W. Ning, C. Zhong, J. He, S. Gong, G. Xie and C. Yang, *Adv. Mater.*, 2019, **31**, 1901404-1901411.

34 M. Zhang, L. Chen, X. Xu, L. Zhao, S. Wang, J. Ding and L. Wang, *J. Mater. Chem. C*, 2019, **7**, 9850-9855.

35 X. Wang, S. Wang, J. Lv, S. Shao, L. Wang, X. Jing and F. Wang, *Chem. Sci.*, 2019, **10**, 2915-2923.

36 P. Y. Vemuri, Y. Wang and F. W. Patureau, *Organic Letters* 2019, **21**, 24, 9856-9859.

37 Q. Zhang, B. Li, S. Huang, H. Nomura, H. Tanaka and C. Adachi, *Nat. Photonics*, 2014, **8**, 326-332.

38 Q. Zhang, D. Tsang, H. Kuwabara, Y. Hatae, B. Li, T. Takahashi, S-Y. Lee, T. Yasuda and C. Adachi, *Adv. Mater.*, 2015, **27**, 2096-2100.

39 W-L. Tsai, M-H. Huang, W-K. Lee, Y-J Hsu, K-C. Pan, Y-H. Huang, H-C. Ting, M. Sarma, Y-Y. Ho, H-C. Hu, C-C. Chen, M-T. Lee, K-T. Wong and C-C. Wu, *Chem. Commun.*, 2015, **51**, 13662-13665.

40 P. Samanta, D. Kim, V. Coropceanu and J. Brédas, *J. Am. Chem. Soc.*, 2017, **139**, 4042−4051.

41 X. Chen, Y. Tsuchiya, Y. Ishikawa, C. Zhong, C. Adachi and J. Brédas, *Adv. Mater.*, 2017, **29**, 1702767.

42 P. Stachelek, J. Ward, P. Dos Santos, A. Danos, M. Colella, N. Haase, S. Raynes, A. Batsanov, M. Bryce and A. Monkman, *ACS Appl. Mater. Interfaces*, 2019, **11**, 27125-27133.

43 J. Ward, N. Kukhta, P. dos Santos, D. Congrave and A. Batsanov, *Chem. Mater.*, 2019, **31**, 6684-6695.

44 D. Zhang, C. Zhao, Y. Zhang, X. Song, P. Wei, M. Cai and Lian Duan, *ACS Appl. Mater. Interfaces* 2017, **9**, 4769−4777.

45 H. Wang, L. Meng, X. Shen, X. Wei, X. Zheng, X. Lv, Y. Yi, Y. Wang and P. Wang, *Adv. Mater.*, 2015, **27**, 4041-4047.

46 D. Di, A. Romanov, L. Yang, J. Richter, J. Rivett, S. Jones, T. Thomas, M. Jalebi, R.

Friend, M. Linnolahti, M. Bochmann and D. Credgington, *Science*, 2017, **356**, 159-163.

47 T. Matulaitis, P. Imbrasas, N. A. Kukhta, P. Baronas, T. Bučiūnas, D. Banevičius, K. Kazlauskas, J. V. Gražulevičius and S. Juršėnas, *J. Phys. Chem. C*, 2017, **121**, 23618-23625.

48 U. Balijapalli, M. Tanaka, M. Auffray, C.-Y. Chan, Y.-T. Lee, Y. Tsuchiya, H. Nakanotani and C. Adachi, *ACS Appl. Mater. Interfaces*, 2020, **12**, 9498-9506.

49 C. Kuei, W. Tsai, B. Tong, M. Jiao, W. Lee, Y. Chi, C. Wu, S. Liu, G. Li and P. Chou, *Adv. Mater.*, 2016, **28**, 2795-2800.

Graphic Abstract

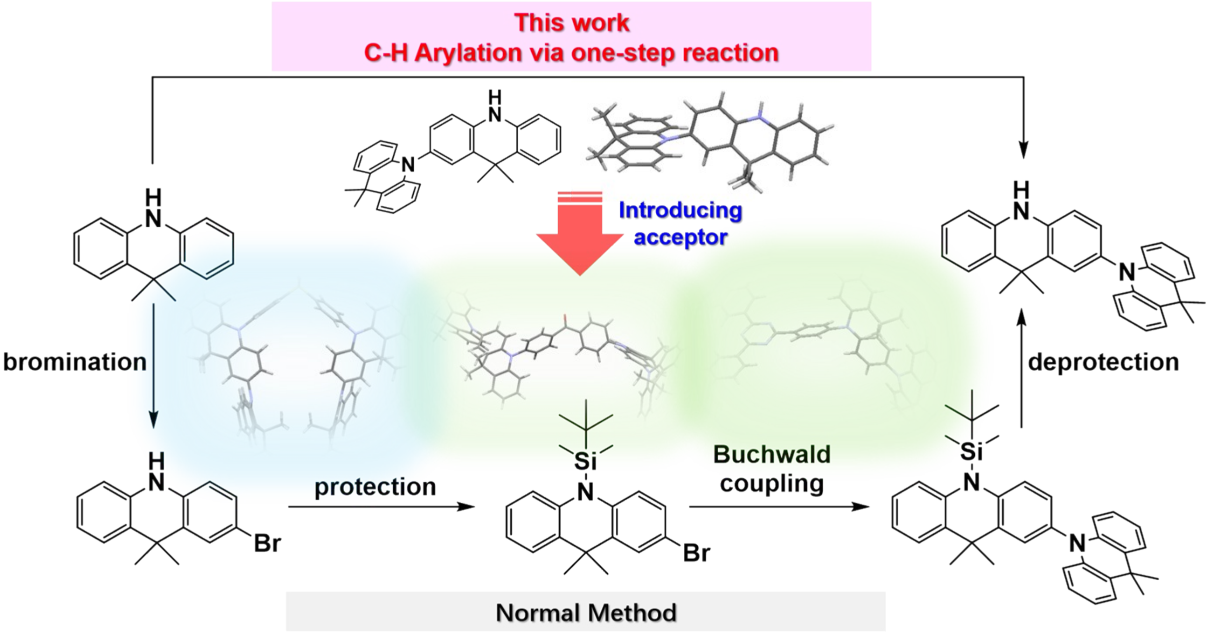

Novel donor fragment of BDMAc is synthesized *via* C-H arylation with one-pot method, and three BDMAc-based TADF molecules are achieved. High emission efficiency of 69-89% are obtained in the solid state. Solution processable OLEDs based on these TADF molecules present high EQE of ～23%.

Supporting Information

Novel Donor Moiety 9,9,9′9′-tetramehtyl-9,9′10,10′-tetrahydro-2,10′-biacridine *Via* One-Pot C-H Arylation for TADF Emitters and Their Application in Highly Efficient Solution-Processable OLEDs

Yuchao Liu, [†‡△] *Zheng Yin,*[†§△] *Xiangbing Wang,*[†△] *Etienne Baranoff,*[#] *Di Zhou,*[†§] *Kai Zhang,*[†]
Zhongjie Ren,[‡*] *Shengyue Wang,*[†] *Weiguo Zhu,*[†*] *Yafei Wang*[†*]

Contents

Experimental Section

Materials and measurements: 9,10-Dihydroacridine, diphenylsulphone, benzophenone and 1,3,5-triazine are commercial from Energy Chemical Company Ltd. Other reagents were purchased from J&K Chemical and Aladdin companies. All reactions were carried out under N_2 atmosphere. ^1H NMR and ^{13}C NMR spectra were acquired using a Bruker Dex-300/400 NMR instrument using $CDCl_3$ as a solvent. Mass spectra (MS) were recorded on a Bruker Autoflex MALDI-TOF instrument using dithranol as a matrix. UV-vis absorption spectra were recorded using a SHIMADZU UV-1650PC. Steady-state photoluminescence (PL) spectra were obtained with a PTI QuantaMaster 40 spectrofluorometer at room temperature and absolute PL quantum yields (PLQY) were recorded using a 3.2 inch integrating sphere. Low temperature photoluminescence spectra were measured using a Jasco FP-6500 at 77 K. Photoluminescence decay traces were obtained through the time correlated single photon counting (TCSPC) techniques by using a PicoQuant, FluoTime 250 instrument (PicoQuant, Germany). A 377 nm pulsed laser was used as an excitation source and data analyses were performed using exponential fitting models by FluoFit software. Thermogravimetric analysis (TGA) was carried out with a NETZSCH STA449 from 25°C to 600°C at a 20°C/min heating rate under N_2 atmosphere. Cyclic voltammetry measurements were performed using a 273A (Princeton Applied Research). Electrochemical property was evaluated by cyclic voltammetry with three typical electrodes in degassed CH_3CN solution with a rate of 100 mV/s. The CV system employed Bu_4NPF_6 as electrolyte. Platinum disk is used as the working electrode, platinum wire is regarded as the counter electrode and silver wire is used as the reference electrode. Ferrocenium/ferrocene (Fc/Fc^+) was used as the external standard compound. Each oxidation potential was calibrated using ferrocene as a reference. LUMO levels were evaluated from the HOMO level and the optical band gap which was obtained from the edge of the absorption spectra. DFT calculations were performed in the gas phase using Gaussian 09 quantum-chemical package. The geometry optimization for ground state of derivatives was carried out using B3LYP functionals with 6-31G (d, p) basis set. TD-DFT calculations were performed using same functional and basis sets that were used. X-ray diffractions of all single crystals were performed at 170 or 296 K on a Bruker Apex II CCD diffractometer using Mo-Kα radiation ($\lambda = 0.71073$ Å). The data integration and scaling were processed with SAINT software, and absorption corrections were performed using the SADABS program. The structures were solved by direct method and refined on F2 by the full-matrix least-squares technique using SHELXL-2014 program package. The remaining hydrogen atoms were placed in calculated positions and refined with a riding model.

Device fabrication and Measurements: The patterned ITO substrates were rinsed with acetone and isopropyl alcohol using sonication for 15 min, followed by 15 min UV-ozone-treatment. After surface treatment, the PEDOT:PSS layer was spin-coated onto the ITO substrate as the hole-injecting layer, and then annealed at 150 ℃ for 15 min. The emissive layers were prepared by spin-coating onto the PEDOT:PSS and then annealed at 80 ^{o}C for 15 min. The hole blocking layer, electron-transporting and the cathode materials were thermally evaporated onto the emitter layer in a vacuum chamber. The thermally evaporated deposition rates are 0.6^{-1} Å s^{-1} for organic layers, 0.1 Å s^{-1} for Liq and 1.5-1.8 Å s^{-1} for Al electrode, respectively. The current-voltage-luminance (J-V-L) characteristics and the electroluminescence spectra of the devices were simultaneously obtained by using a spectroradiometer (PR735) and Keithley 2400 sourcemeter unit under ambient atmosphere at room temperature.

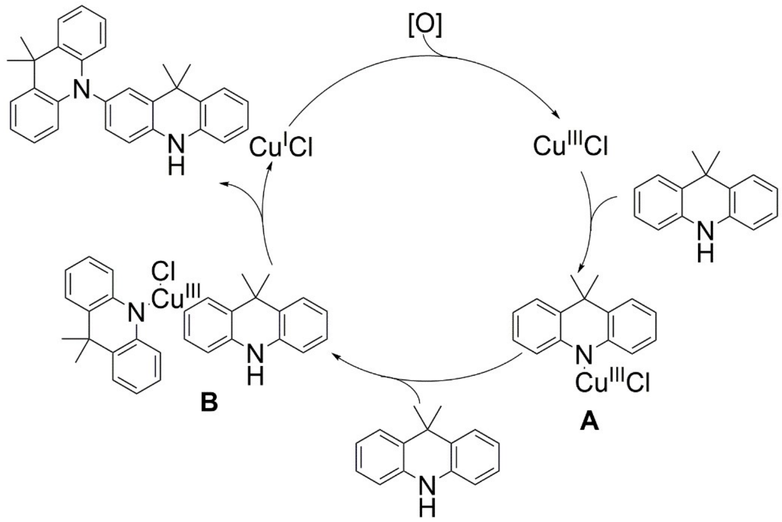

Scheme S1. Potential mechanism for the BDMAc

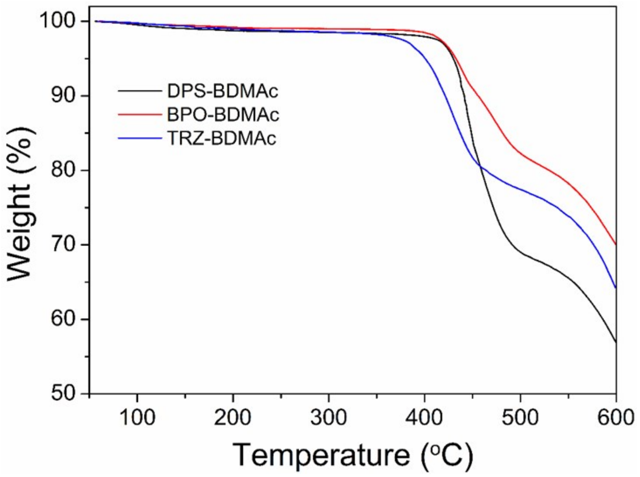

Figure S1. TGA curves of compounds under N_2 with a rate of 20 ^{o}C/min

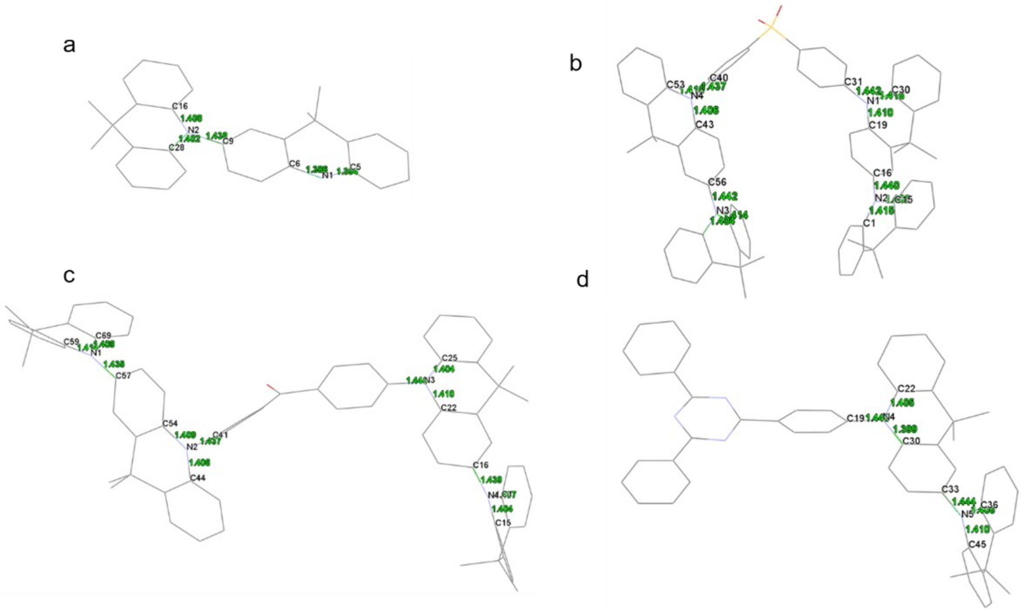

Figure S2. Crystal structures with partial bond lengths of TADF emitters.

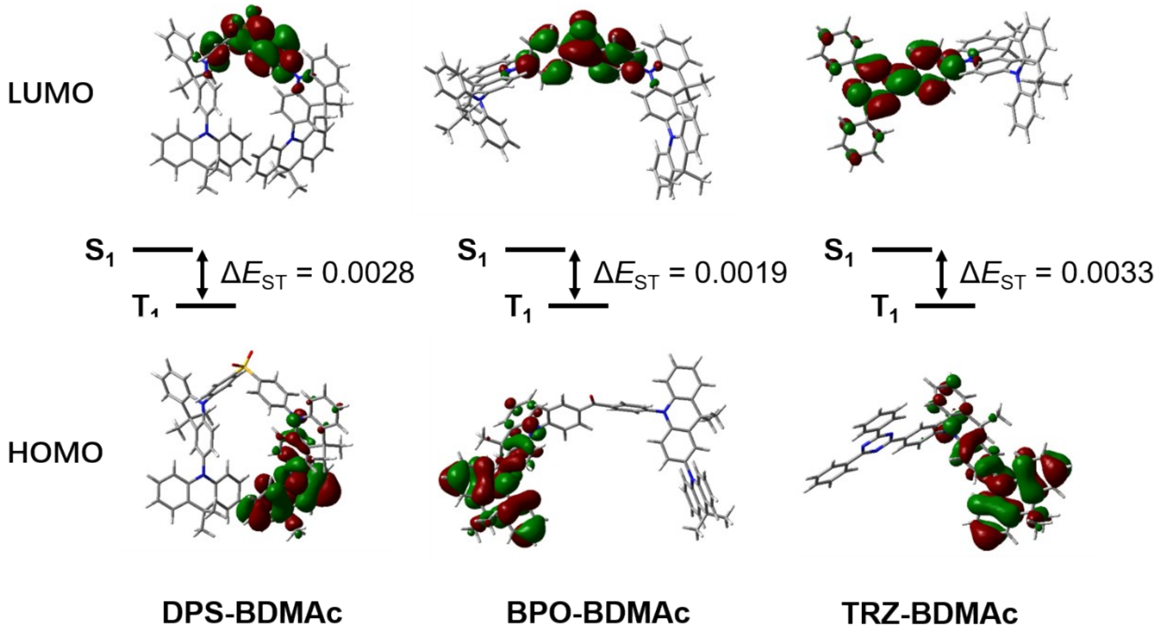

Figure S3. Molecular structures and HOMO and LUMO distributions based on ground state (S_1) at the B3LYP/6-31G(d) level for compounds; the excitation energies of singlet (S_1) and triplet (T_1) were evaluated by TD-DFT/BMK/6-31G(d) based on the optimized S_1 geometry.

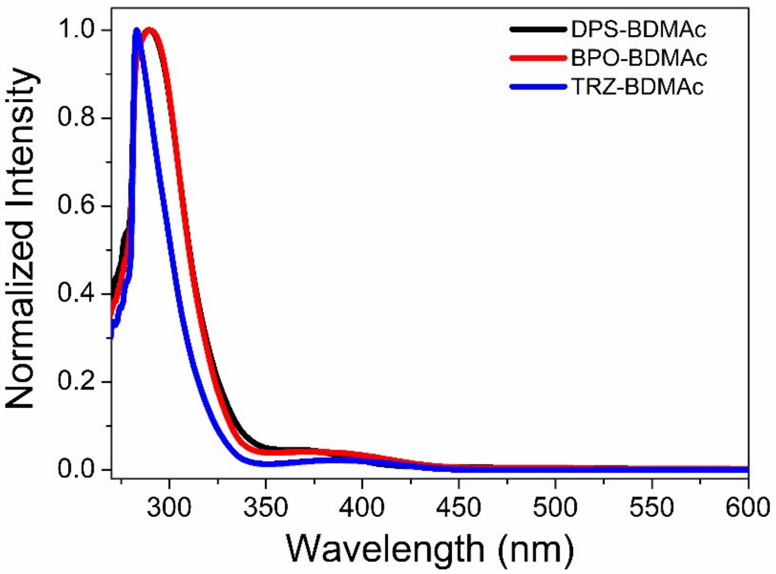

Figure S4. UV-absorption spectra of compounds in toluene solution

Table S5. The comparison of properties between molecules obtained in this work and the molecules without substituent group located at 2-position of acridine.

Emitters	ΔE_{ST} [meV][a]	λ_{em} [nm][b]	Φ_{PL} [%][c]	τ_p [ns][d]	τ_d [μs][e]	EQE_{max} [%]	*ref*
DPS-DMAC	90	464	80	21	3.1	19.5[f]	1
DPS-BDMAC	20	481	69.1	32.6	2.1	12.35[g]	This work
BP-DMAC	80	506	90	19.3	3.0	18.9[f]	2
BPO-BDMAC	30	516	89.1	44.9	3.0	22.53[g]	This work
TRZ-DMAC	50	495	90	20.3	1.9	26.5[f]	3
TRZ-BDMAC	40	510	87	36.5	2.8	13.86[g]	This work

[a] the singlet and triplet energy splitting value obtained in toluene; [b] maximum emission peaks of doped films; [c] photoluminescence quantum efficiency of doped film under nitrogen atmosphere; [d] lifetime of prompt fluorescence of doped film; [e] lifetime of delayed fluorescence of doped film; [f] maximum external quantum efficiency of vacuum-deposited devices; [g] maximum external quantum efficiency of solution-processed devices.

[redacted]

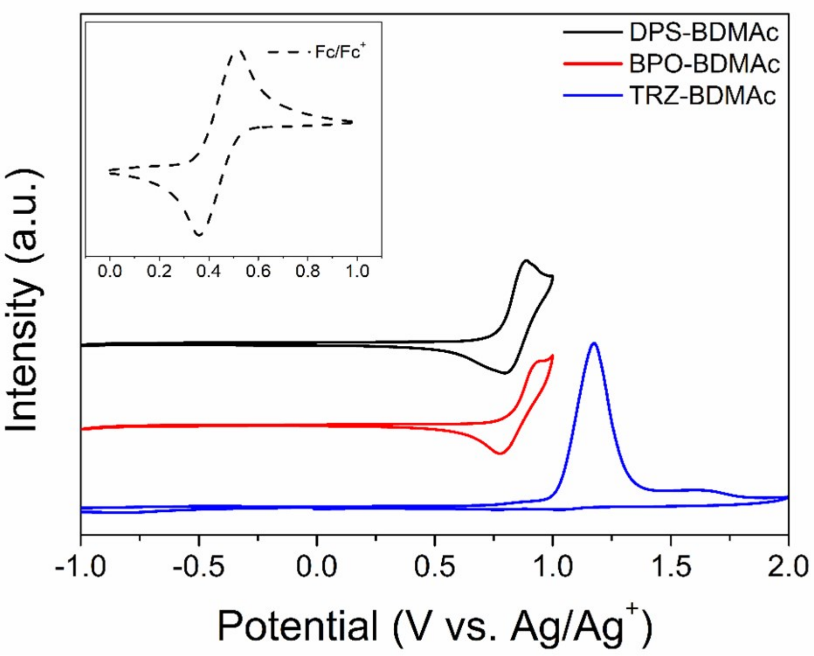

Figure S5. CV curves of compounds under N_2 in CH_3CN solution

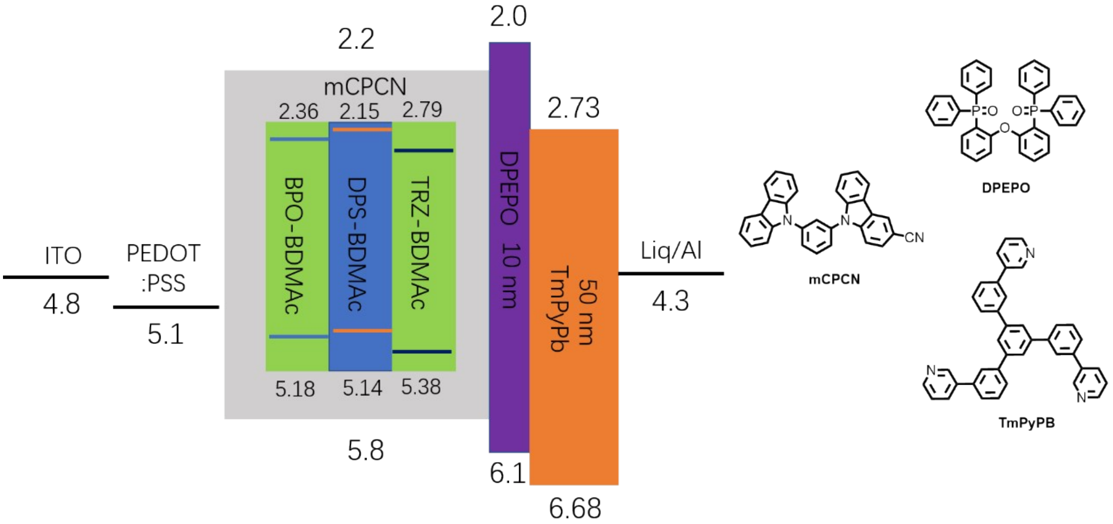

Figure S6 Relative energy levels and molecular structures of materials used in devices

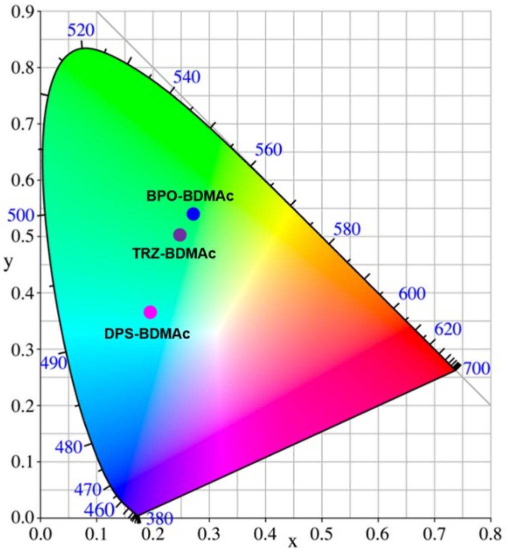

Figure S7. CIE coordinates of the devices.

Quantum efficiencies and decay rate constants

Based on the Φ_{PL} and lifetime, the photophysical constants were calculated according to the formulae (S1)～(S6):

$$k_p = \frac{1}{\tau_p} \qquad \text{(S1)}$$

$$k_{rISC} = \frac{k_p k_d \Phi_d}{k_{ISC} \Phi_p} \qquad \text{(S2)}$$

$$k_d = \frac{1}{\tau_d} \qquad \text{(S3)}$$

$$k_r = \frac{\Phi_p}{\tau_p} \qquad \text{(S4)}$$

$$k_{ISC} = \frac{\Phi_d}{\Phi_{PL} \tau_p} \qquad \text{(S5)}$$

$$k_{nr} = k_r \frac{1 - \Phi}{\Phi} \qquad \text{(S6)}$$

Herein, k_r and k_{nr} denote radiative and nonradiative decay rate constant from S_1 to S_0, respectively. The k_p is intersystem crossing (k_{ISC}), while k_{rISC} is the reverse intersystem crossing between the S_1 and T_1. Φ is the total photoluminescent quantum yield. Φ_p and Φ_d are the prompt and delayed luminescence quantum efficiency, respectively. τ_p and τ_d, the lifetime of prompt and delayed components.

References

[1] Q. Zhang, B. Li, S. Huang, H. Nomura, H. Tanaka, C. Adachi, Efficient blue organic light-emitting diodes employing thermally activated delayed fluorescence. *Nat. Photonics*, 2014, **8**, 326-332.

[2] Q. Zhang, D. Tsang, H. Kuwabara, Y. Hatae, B. Li, T. Takahashi, S-Y. Lee, T. Yasuda, C. Adachi, Nearly 100% internal quantum efficiency in undoped electroluminescent devices employing pure organic emitters. *Adv. Mater.*, 2015, **27**, 2096-2100.

[3] W-L. Tsai, M-H. Huang, W-K. Lee, Y-J Hsu, K-C. Pan, Y-H. Huang, H-C. Ting, M. Sarma, Y-Y. Ho, H-C. Hu, C-C. Chen, M-T. Lee, K-T. Wong, C-C. Wu, A versatile thermally activated delayed fluorescence emitter for both highly efficient doped and non-doped organic light emitting devices. *Chem. Commun.*, 2015, **51**, 13662-13665.

Table S1 Crystal data and structure refinement for BDMAc

Empirical formula	$C_{30}H_{28}N_2$
Formula weight	416.54
Temperature/K	173.0
Crystal system	monoclinic
Space group	$P2_1/n$
a/Å	9.3201(11)
b/Å	8.8662(10)
c/Å	27.185(3)
α/°	90.00
β/°	94.041(3)
γ/°	90.00
Volume/Å^3	2240.8(4)
Z	4
ρ_{calc}g/cm^3	1.235
μ/mm^{-1}	0.072
F(000)	888.0
Crystal size/mm^3	0.15 × 0.08 × 0.06
Radiation	MoKα (λ = 0.71073)
2Θ range for data collection/°	4.54 to 52.94
Index ranges	$-10 \leq h \leq 11$, $-11 \leq k \leq 11$, $-34 \leq l \leq 33$
Reflections collected	15962
Independent reflections	4516 [R_{int} = 0.0550, R_{sigma} = 0.0556]
Data/restraints/parameters	4516/0/297
Goodness-of-fit on F^2	1.027
Final R indexes [I>=2σ (I)]	R_1 = 0.0510, wR_2 = 0.1196
Final R indexes [all data]	R_1 = 0.0813, wR_2 = 0.1375
Largest diff. peak/hole / e Å^{-3}	0.21/-0.22

Table S2 Crystal data and structure refinement for DPS-DMAc

Empirical formula	$C_{72}H_{62}N_4O_2S$
Formula weight	1047.31
Temperature/K	150.0
Crystal system	monoclinic
Space group	$P2_1/c$
a/Å	12.0494(3)
b/Å	34.7102(12)
c/Å	15.7587(5)
α/°	90
β/°	98.2790(10)
γ/°	90
Volume/Å^3	6522.2(3)
Z	4
ρ_{calc}g/cm^3	1.067
μ/mm^{-1}	0.095
F(000)	2216.0
Crystal size/mm^3	0.19 × 0.12 × 0.08
Radiation	MoKα (λ = 0.71073)
2Θ range for data collection/°	4.384 to 52.798
Index ranges	$-12 \leq h \leq 15$, $-43 \leq k \leq 39$, $-19 \leq l \leq 19$
Reflections collected	56832
Independent reflections	13263 [R_{int} = 0.0569, R_{sigma} = 0.0533]
Data/restraints/parameters	13263/0/720
Goodness-of-fit on F^2	1.016
Final R indexes [I>=2σ (I)]	R_1 = 0.0613, wR_2 = 0.1536
Final R indexes [all data]	R_1 = 0.1012, wR_2 = 0.1765
Largest diff. peak/hole / e Å^{-3}	0.36/-0.28

Table S3 Crystal data and structure refinement for BPO-BDMAc

Empirical formula	$C_{74}H_{64}Cl_2N_4O$
Formula weight	1096.19
Temperature/K	170.15
Crystal system	monoclinic
Space group	$P2_1/n$
a/Å	23.2684(10)
b/Å	8.0445(4)
c/Å	31.1544(13)
α/°	90
β/°	94.1100(10)
γ/°	90
Volume/Å^3	5816.6(5)
Z	4
ρ_{calc}g/cm^3	1.252
μ/mm^{-1}	0.162
F(000)	2312.0
Crystal size/mm^3	0.05 × 0.02 × 0.01
Radiation	MoKα (λ = 0.71073)
2Θ range for data collection/°	5.23 to 52.758
Index ranges	$-28 \leq h \leq 29$, $-10 \leq k \leq 10$, $-36 \leq l \leq 38$
Reflections collected	61525
Independent reflections	11850 [R_{int} = 0.0691, R_{sigma} = 0.0580]
Data/restraints/parameters	11850/0/738
Goodness-of-fit on F^2	1.020
Final R indexes [I>=2σ (I)]	R_1 = 0.0642, wR_2 = 0.1540
Final R indexes [all data]	R_1 = 0.1189, wR_2 = 0.1788
Largest diff. peak/hole / e Å^{-3}	0.31/-0.57

[redacted]

Table S4 Crystal data and structure refinement for TRZ-BDMAc

Empirical formula	$C_{52}H_{43}Cl_2N_5$
Formula weight	808.81
Temperature/K	170.0
Crystal system	monoclinic
Space group	C2/c
a/Å	59.7302(19)
b/Å	8.9036(3)
c/Å	54.0886(19)
α/°	90
β/°	119.0850(10)
γ/°	90
Volume/Å^3	25137.8(15)
Z	24
ρ_{calc}g/cm^3	1.282
μ/mm^{-1}	0.198
F(000)	10176.0
Crystal size/mm^3	0.08 × 0.05 × 0.04
Radiation	MoKα (λ = 0.71073)
2Θ range for data collection/°	4.422 to 51.422
Index ranges	$-72 \leq h \leq 72$, $-10 \leq k \leq 10$, $-65 \leq l \leq 65$
Reflections collected	132351
Independent reflections	23853 [R_{int} = 0.1035, R_{sigma} = 0.0782]
Data/restraints/parameters	23853/0/1606
Goodness-of-fit on F^2	1.020
Final R indexes [I>=2σ (I)]	R_1 = 0.0728, wR_2 = 0.1694
Final R indexes [all data]	R_1 = 0.1375, wR_2 = 0.2033
Largest diff. peak/hole / e Å^{-3}	1.40/-1.27

[redacted]

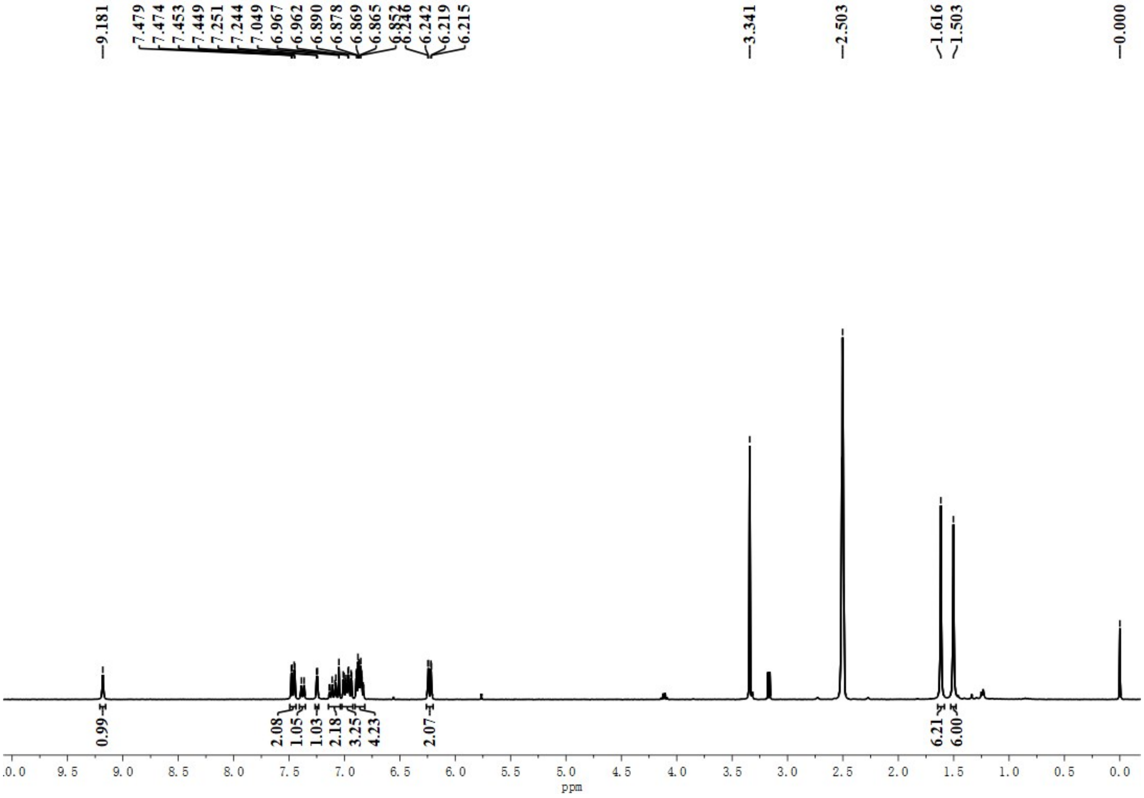

^{1}H NMR spectrum of BDMAc in CDCl$_3$

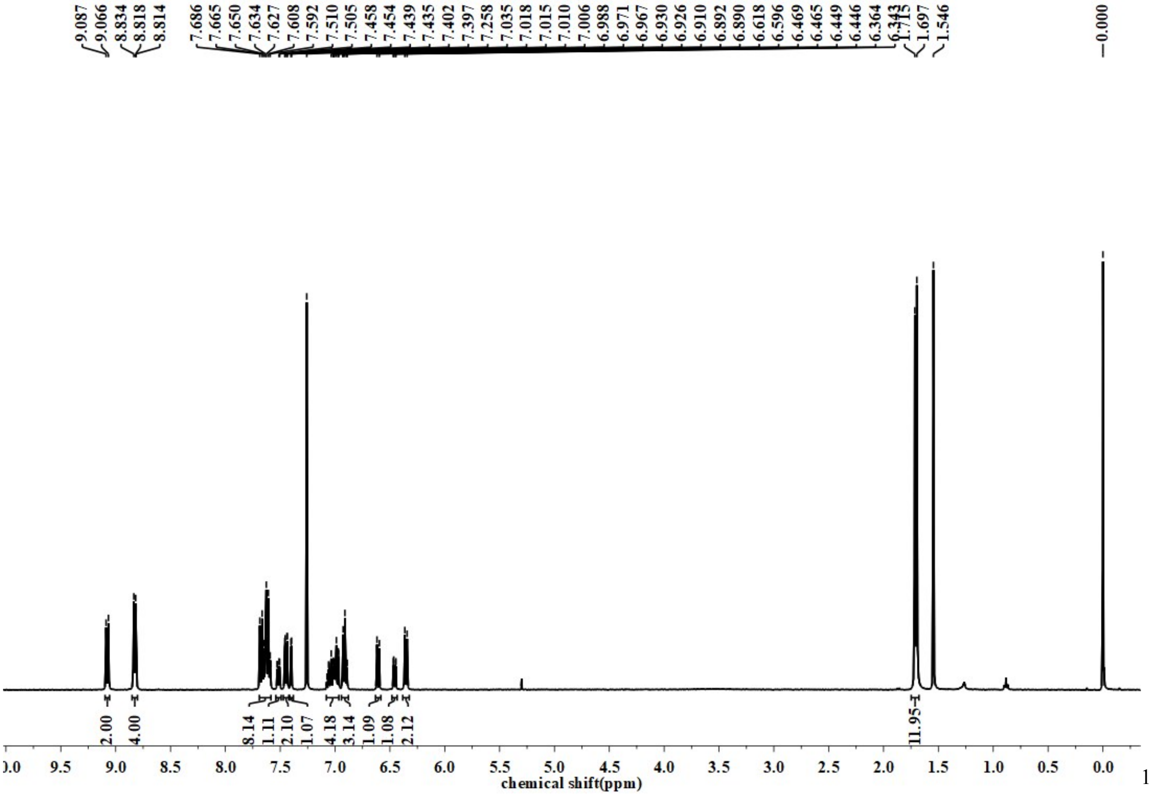

^{1}H NMR spectrum of TRZ-BDMAc in CDCl$_3$

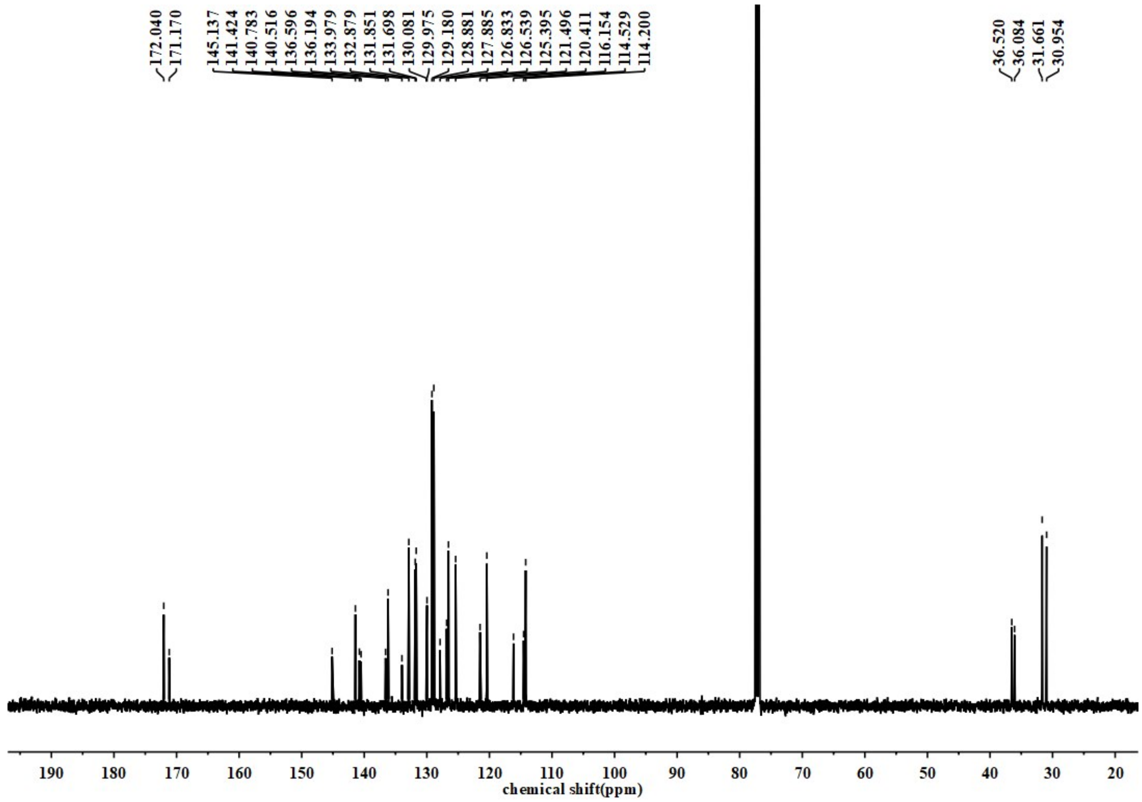

^{13}C NMR spectrum of TRZ-BDMAc in $CDCl_3$

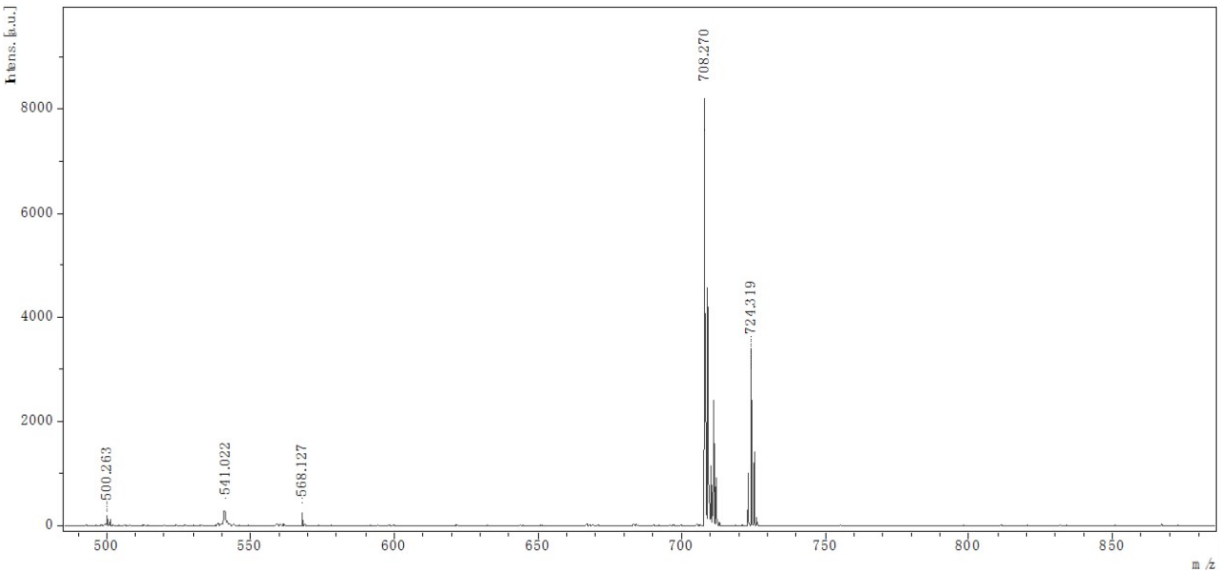

TOF-MS spectrum of TRZ-BDMAc

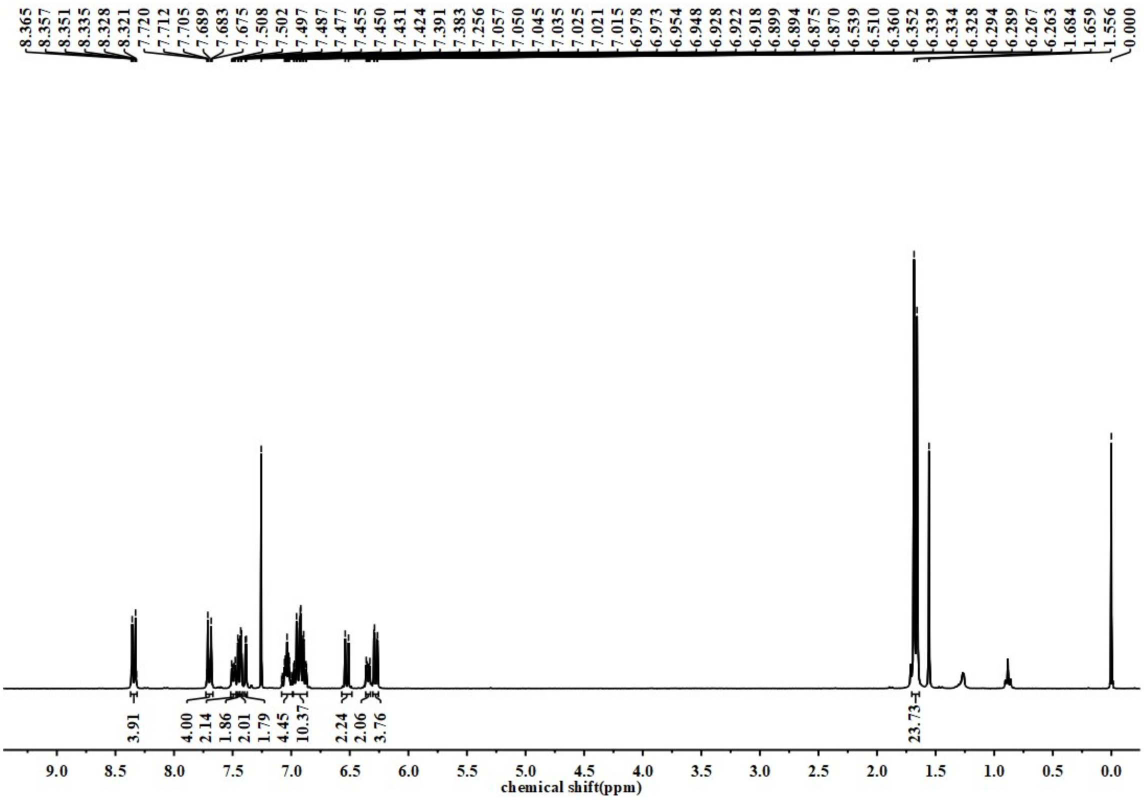

^{1}H NMR spectrum of DPS-BDMAc in $CDCl_3$

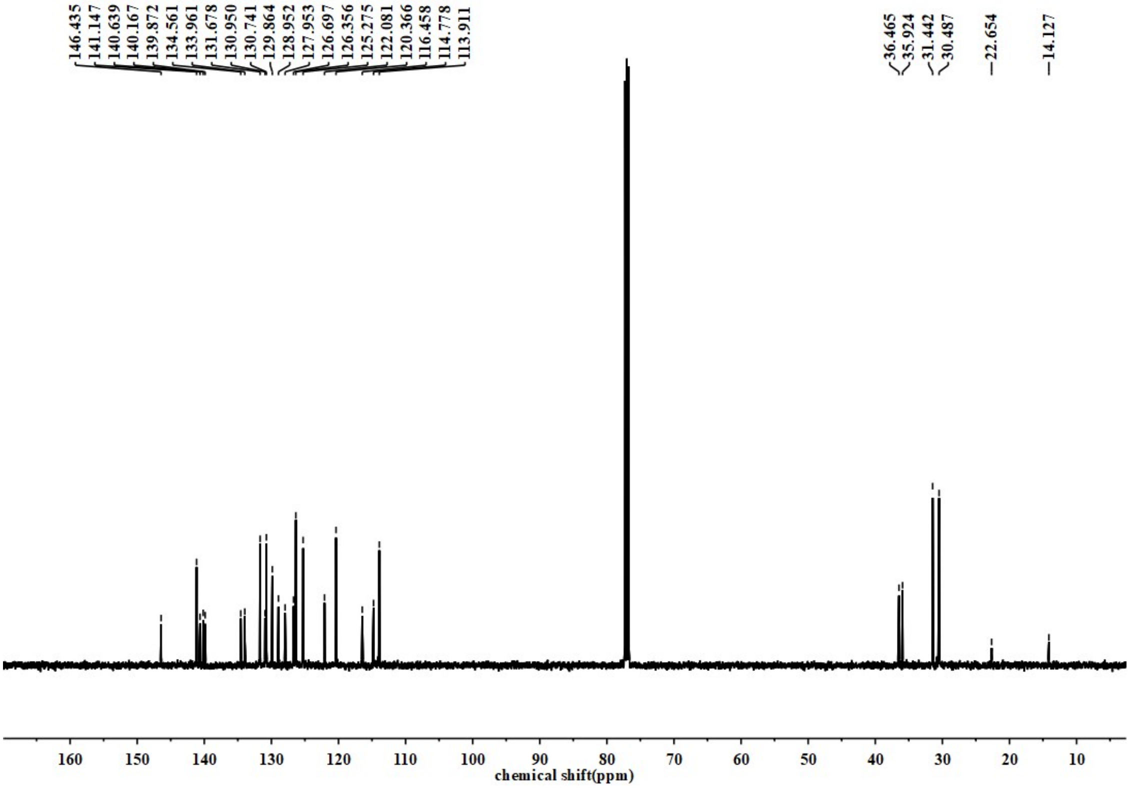

^{13}C NMR spectrum of DPS-BDMAc in $CDCl_3$

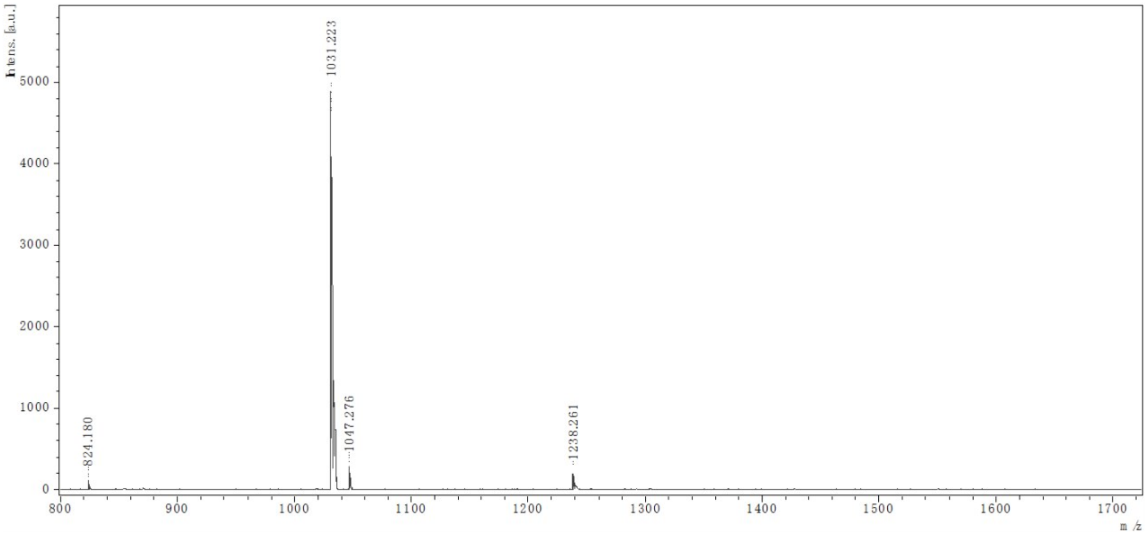

TOF-MS spectrum of DPS-BDMAc

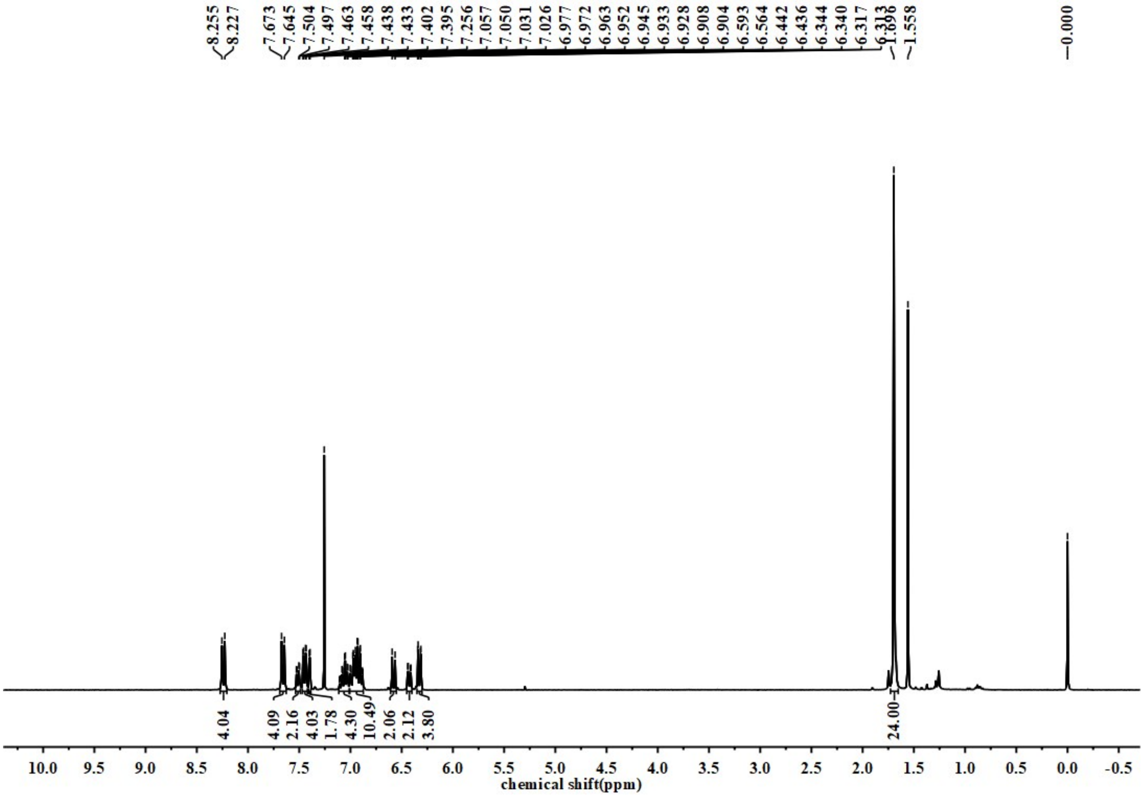

^{1}H NMR spectrum of BPO-BDMAc in $CDCl_3$

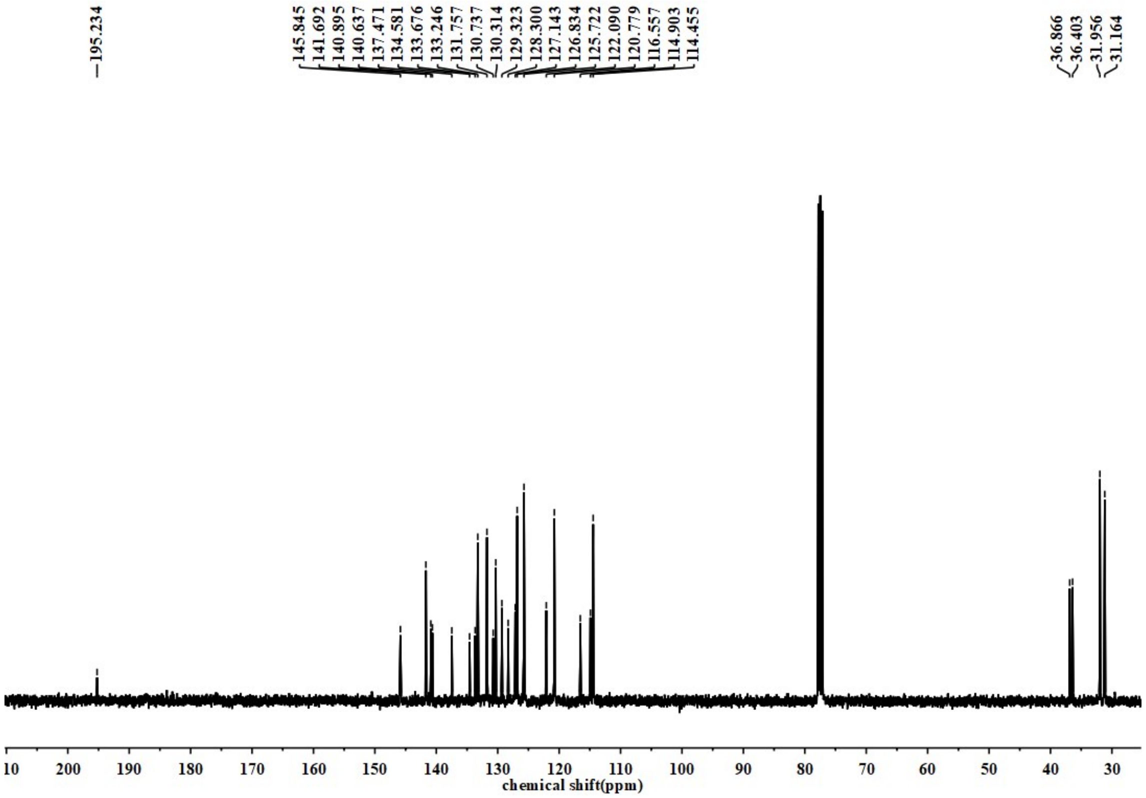

^{13}C NMR spectrum of BPO-BDMAc in CDCl$_3$

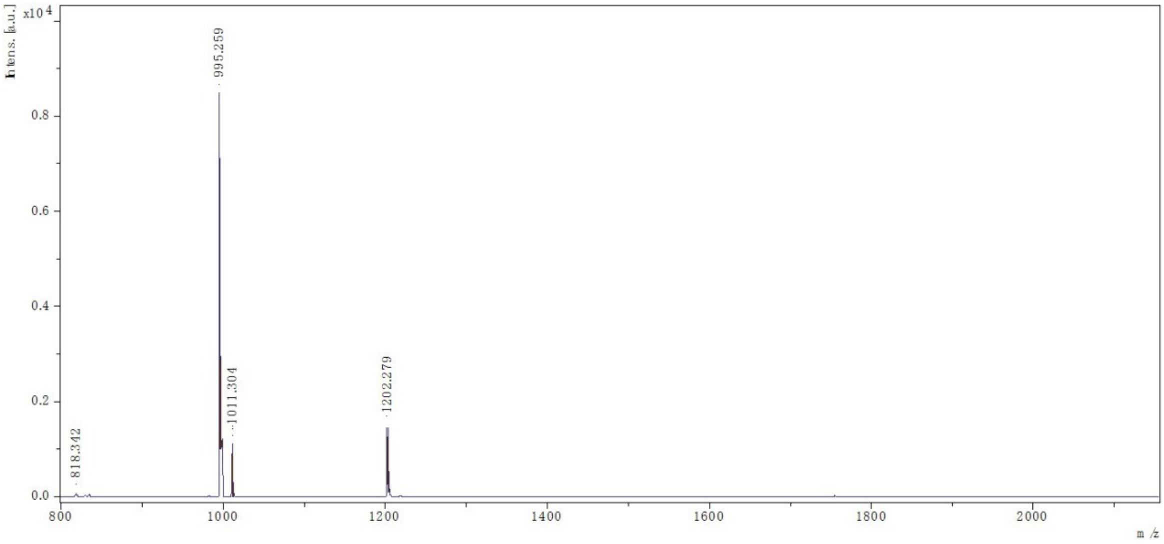

TOF-MS spectrum of BPO-BDMAc